AD-A069 208 AUBURN UNIV ALA ENGINEERING EXPERIMENT STATION F/G 9/3
CORRELATION ALGORITHM DEVELOPMENT.(U)
APR 79 J S BOLAND, H S RANGANATH DAAK40-79-M-0016
UNCLASSIFIED NL

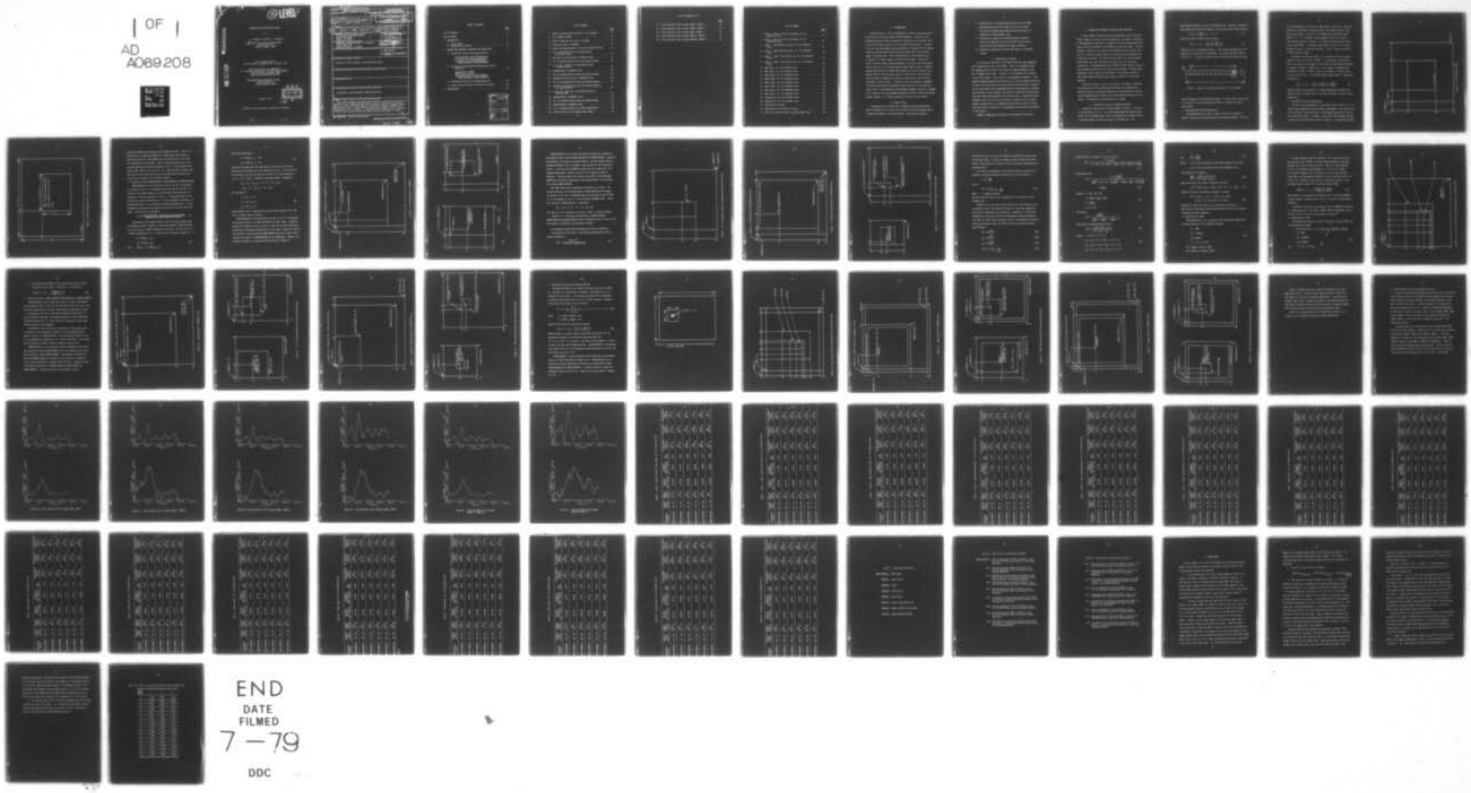

END
DATE FILMED
7-79
DDC

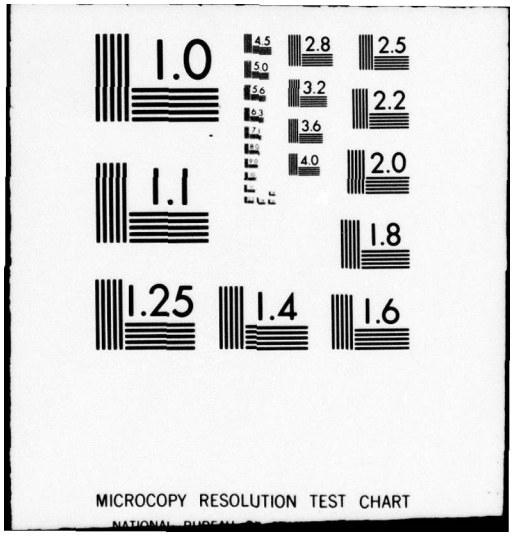
1.0
1.1
1.25
1.4
1.6
1.8
2.0
2.2
2.5
2.8
3.2
3.6
4.0
4.5
5.0
5.6
6.3
MICROCOPY RESOLUTION TEST CHART

CORRELATION ALGORITHM DEVELOPMENT

by

J. S. Boland, III and H. S. Ranganath

Electrical Engineering Department
Auburn University
Auburn, Alabama 36830

Final Technical Report
For the Period 1 December 1978 - 30 April 1979

This research work was supported by
U.S. Army Missile Research and Development Command
Redstone Arsenal, Alabama 35809
under Contract DAAK40-79-M-0016

ENGINEERING EXPERIMENT STATION
Auburn University
Auburn, Alabama 36830

30 April 1979

SECURITY CLASSIFICATION OF THIS PAGE (When Data Entered)

REPORT DOCUMENTATION PAGE	READ INSTRUCTIONS BEFORE COMPLETING FORM
1. REPORT NUMBER	2. GOVT ACCESSION NO. 3. RECIPIENT'S CATALOG NUMBER
4. TITLE (and Subtitle) (6) CORRELATION ALGORITHM DEVELOPMENT.	(9) Final technical rept. 5. TYPE OF REPORT & PERIOD COVERED 1 Dec 78-30 Apr 79
	6. PERFORMING ORG. REPORT NUMBER
7. AUTHOR(s) (10) J. S. Boland, III H. S. Ranganath	8. CONTRACT OR GRANT NUMBER(s) (15) DAAK40-79-M-0016
9. PERFORMING ORGANIZATION NAME AND ADDRESS Engineering Experiment Station Auburn University Auburn, AL 36830	10. PROGRAM ELEMENT, PROJECT, TASK AREA & WORK UNIT NUMBERS (12) 70p.
11. CONTROLLING OFFICE NAME AND ADDRESS Commander, US Army Missile R & D Command ATTN: DRDMI-TGC Redstone Arsenal, AL 35809	12. REPORT DATE (11) 30 Apr 79 13. NUMBER OF PAGES 68
14. MONITORING AGENCY NAME & ADDRESS (if different from Controlling Office)	15. SECURITY CLASS. (of this report) UNCLASSIFIED 15a. DECLASSIFICATION/DOWNGRADING SCHEDULE

16. DISTRIBUTION STATEMENT (of this Report)

Cleared for Public Release; Distribution Unlimited

17. DISTRIBUTION STATEMENT (of the abstract entered in Block 20, if different from Report)

18. SUPPLEMENTARY NOTES

19. KEY WORDS (Continue on reverse side if necessary and identify by block number)

Correlation, Target Hand-Off, Image Correlation

20. ABSTRACT (Continue on reverse side if necessary and identify by block number)

This report presents the results and conclusions derived from simulation of correlation of TV images obtained from two sensors sensitive in the visual spectrum. Eight scenes were used with a variety of spatial frequency content and contrast ratios. Three methods of obtaining a threshold for bi-level quantization are also studied. A comparison of the shapes of the correlation surfaces about the true correlation peak and about false peaks is given.

DD FORM 1 JAN 73 1473 EDITION OF 1 NOV 65 IS OBSOLETE

SECURITY CLASSIFICATION OF THIS PAGE (When Data Entered)

TABLE OF CONTENTS

LIST OF FIGURES

LIST OF FIGURES (Con't)

LIST OF TABLES

1. INTRODUCTION

Currently the U.S. Army is developing a system for the acquisition and tracking of military targets from helicopters. The Army is also developing missiles which are capable of locking on to the target prior to launch and then of homing in on the target during flight. To accomplish this task some means must be provided for "handing off" the target from the precision pointing and tracking system (PTS) to the missile seeker in minimum time. The PTS can either be a high resolution day TV system or a forward looking infrared (FLIR) system. The missile, which is usually lower resolution because of size and costs constraints, can be a day TV or an infrared imaging seeker (IRIS) system. Therefore target hand-off must be accomplished between two similar sensors (e.g., between the PTS high resolution day TV and the missile low resolution day TV system) or between two dissimilar sensors (e.g., the PTS high resolution TV and an IRIS). In order to study the sensitive parameters in existing techniques to accomplish target hand-off in the above two cases, the U.S. Army Research and Development Command, Huntsville, Alabama, let a contract with the Engineering Experiment Station, Auburn University, Auburn, Alabama. This report presents the results of that effort.

A. Scope of Work

The purpose of this study was to determine the optimal gradient matrix thresholds for bi-level and tri-level correlation between two TV systems and between a TV and IRIS system. This analysis required

1) Establishing 3 x 3 gradient matrices utilizing the SOBEL edge detection concept for eight (8) IR and TV scenes. The digitized images were supplied by the government on standard nine track magnetic tape.
2) Performing an analysis to determine optimal threshold values for generation of bi-level and tri-level correlation matrices which maximize the image correlation.
3) Performing simulations to verify the results in paragraph 2 above.

B. Organization of Report

All of the work outlined in the Scope of Work has been completed and is documented in this final report. Task 1 in the Scope of Work was completed and the results are stored in computer memory on Disk and in computer print-outs. The data is too voluminous for inclusion in this final report. Tasks 2 and 3 are documented in Chapter 2. The optimal threshold problem for bi-level and tri-level correlation matrices is similar for both the TV-to-TV and the TV-to-IR correlation. Because of the large amount of data generated and the limited amount of computer time available on this contract, the TV-to-TV correlation only was simulated and results extrapolated to the TV-to-IR case. Simulations using reference sizes of 32 x 32, 16 x 16 and 8 x 8 were run for all cases. However, because the 8 x 8 references did not lead to correct correlation, only the 32 x 32 and 16 x 16 reference array results are presented in this report.

Chapter 3 summarizes the results and conclusions of the work.

2. CORRELATION THRESHOLD TECHNIQUES AND SIMULATION

In this chapter, three preprocessing algorithms used to transform digital images to a binary form are presented. The spatial resolution of High Resolution (HR) Video is reduced to that of Low Resolution (LR) Video, before the HR-Video is transformed to the binary form. The difference in resolution is caused by the differing fields of view, number of TV lines per frame, frame rate, aspect ratio and sampling rate of the two TV systems. The vertical scale factor, W_V, and horizontal scale factor, W_H, were previously calculated to be 3.32 and 6.64, respectively. Preprocessed HR and LR videos in binary form are input to the correlation process and the results are tabulated. The algorithms discussed in this chapter are applicable to a correlator system in which both images are acquired with sensors sensitive in the visual spectrum.

For Scene 3 (jeep in front of the fence), the method of choosing the reference array from preprocessed HR-Video, the technique for generating various correlation surfaces and the technique for calculating the expected peak locations in the correlation surfaces are illustrated. Final results are tabulated for all scenes.

A. Correlation Using Line Average Quantizer

Consider a single line of video as shown in Figure 1. The pixel to be quantized is X(i,j). The line average quantizer quantizes the points of the selected input array by calculating the average value of a specified number of previous pixels of the same line. The

quantization threshold is then this average value. Equation 1 describes the average value calculation where L is the average Value Sample Length.

$$\overline{X}(i,j) = \frac{1}{L} \sum_{J=1}^{L} X(i, j - J + 1) \qquad (1)$$

Equation 2 gives the quantization process

$$X_q(i, j) = \begin{cases} 1 & ; \quad X(i, j) \geq \overline{X}(i, j) \\ 0 & ; \quad X(i, j) < \overline{X}(i, j) \end{cases} \qquad (2)$$

where $X_q(i, j)$ is the quantized pixel. This process continues until all pixels in the input array are quantized. As can be seen from Figure 1, the first (L - 1) pixels of each line will be quantized incorrectly and

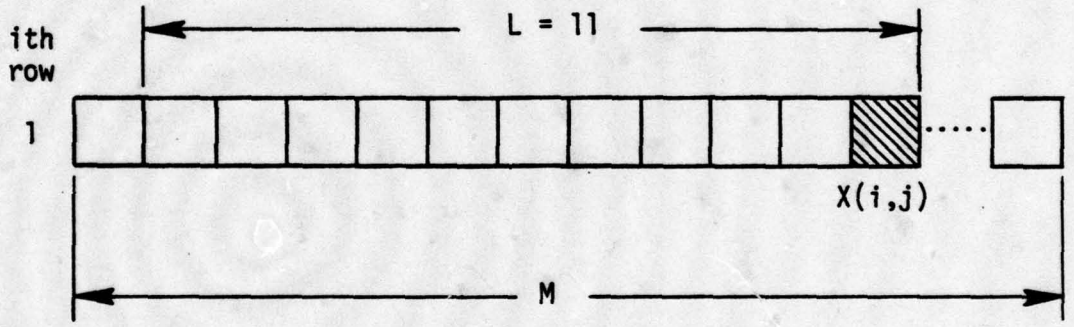

Figure 1. Layout for quantization based on a line average.

must be ignored in the correlation process. If the original input array is of size N x M, then the quantized array will contain N x (M-L+1) valid points.

1. High Resolution Video Preprocessing

As mentioned earlier, Scene 3 (jeep in front of the fence) is used to illustrate the preprocessing and correlation process. The size

of the unprocessed high resolution video (UHRV) is 240 x 512. When the resolution of HR-Video is reduced to that of LR-Video by using the W_H and W_V scale factors, the size of the reduced high resolution video (RHRV) is 72 x 77. The RHRV is then quantized line by line using a line average quantizer of length 11, to obtain the processed high resolution video (PHRV). A reference array (REFV) of size 32 x 32, which includes the jeep, is selected from PHRV. Figure 2 shows the position of PHRV and REFV in RHRV.

For better correlation results, it is necessary to have an equal number of 'ones' and 'zeros' in REFV. If, in the REFV, the number of ones is not equal to the number of zeros ±5%, the quantization threshold is changed, and RHRV is requantized. This process is repeated until the number of 'ones' in REFV is equal to the number of 'zeros' within the limit of ±5% error. The modified quantization process is described by Equation 3.

$$X_q(i, j) = \begin{cases} 1 & ; \quad X(i, j) \geq \overline{X}(i, j) + \text{DELTA} \\ 0 & ; \quad X(i, j) < \overline{X}(i, j) + \text{DELTA} \end{cases} \qquad (3)$$

Obviously DELTA can be positive or negative depending on whether the number of ones is greater than or less than the number of zeros in REFV, respectively.

2. Low Resolution Video Preprocessing

The size of the unprocessed low resolution video is 240 x 512. In order to save computation time and memory requirements, only that portion of the LR Video as described below is preprocessed and used as input to the correlation process. A segment of size 120 x 240 including the jeep is chosen from the LR Video as shown in Figure 3. The sampling frequency

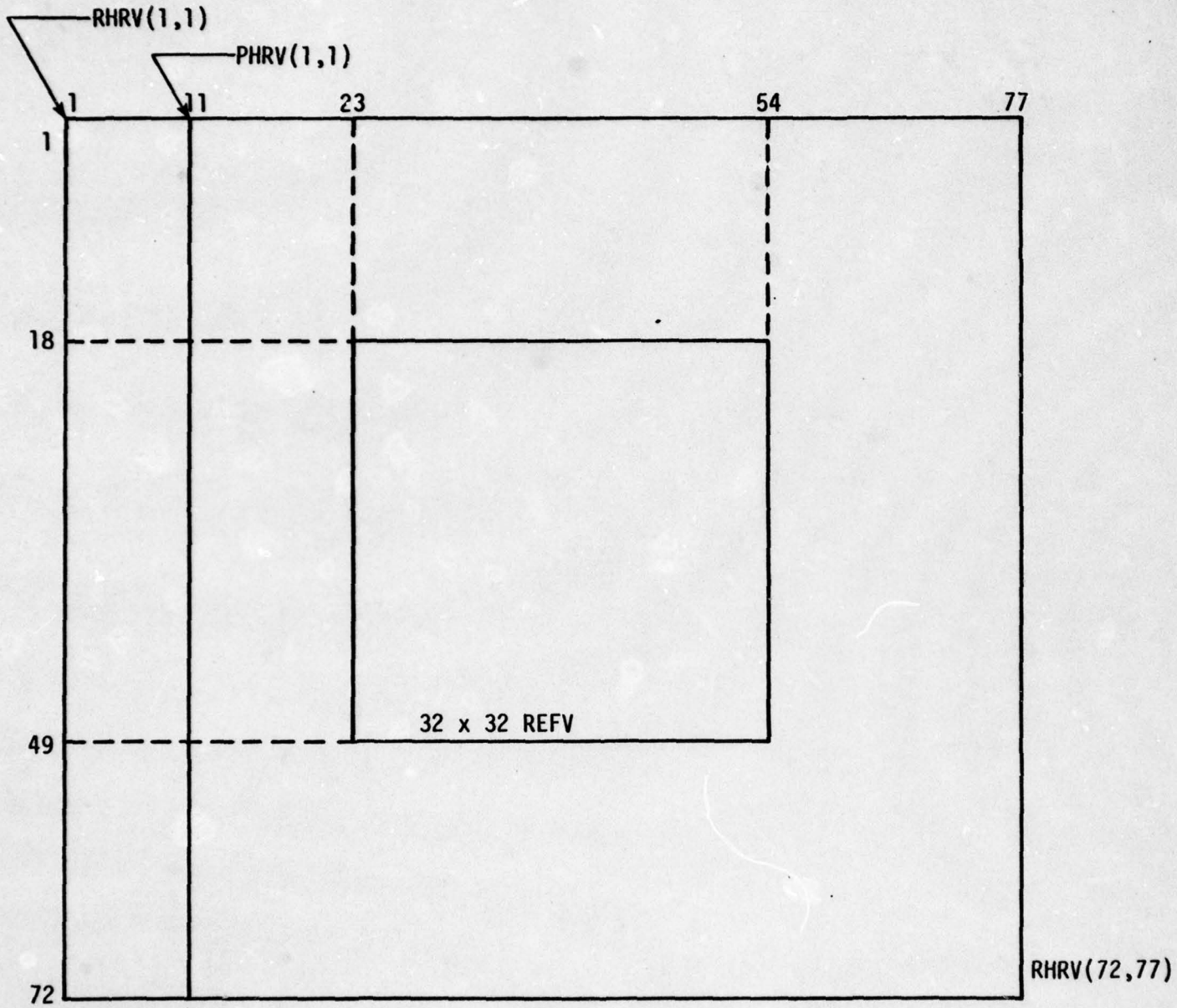

Figure 2. 32 x 32 REFV in RHRV.

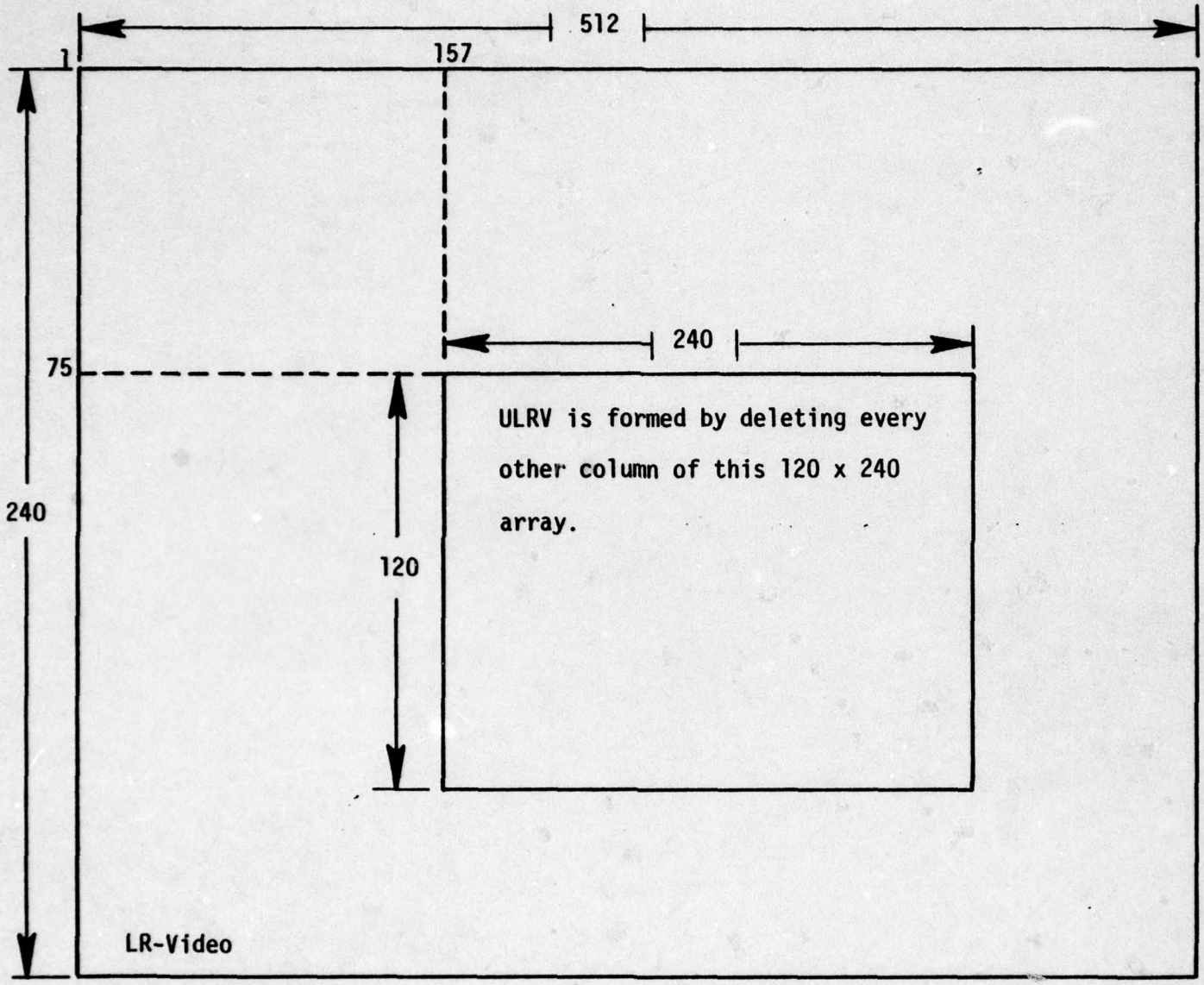

Figure 3. ULRV of dimension 120 x 120 in LR-Video.

used while forming the original digital image was 10 MHz. Since it is desired to use a sampling frequency of 5 MHz, every other column is deleted from the 120 x 240 segment and the resulting 120 x 120 video will henceforth be called ULRV. ULRV is then quantized using a line average quantizer described by Equations 1 and 2. The processed binary form of ULRV, PLRV, is of size 120 x 110. PLRV and PHRV in binary form are input to the correlation process to generate the correlation surfaces to be discussed in the following sections.

3. Correlation Arrays EED28.CORJ3A32, EED28.CORJ3B32 and EED28.CORJ3C32

EED28.CORJ3A32 is the correlation array of size 89 x 79 obtained by correlating the 32 x 32 reference array with PLRV of size 120 x 110. The first four highest peaks of the correlation surface and their coordinates in PLRV are tabulated in Table 1. The average value of the correlation surface excluding the 7 x 7 array centered at the peak, the standard deviation of the correlation surface excluding the 7 x 7 array centered at the peak and the signal-to-noise (S/N) ratio are also computed. The S/N ratio is defined as

$$S/N = \frac{\text{Correlation Peak - Correlation Surface Average}}{\text{Correlation Surface Standard Deviation}} \qquad (4)$$

Coordinates of the expected peak in the correlation surface were calculated by visual inspection of overstruck images of RHRV and PLRV. Let P_1 be a pixel in RHRV, preferably on the jeep, and P_2 be the pixel in ULRV corresponding to P_1 in RHRV which was located by inspection. If

$$P_1 = RHRV(I_1, J_1),$$

$$P_2 = ULRV(I_2, J_2), \qquad (5)$$

and $$REFV(1, 1) = PHRV(K_2, L_2)$$

then after quantization

$$P_1 = PHRV(I_1, J_1 - 10)$$
$$P_2 = PLRV(I_2, J_2 - 10) \quad (6)$$

Since ULRV and RHRV have the same spatial resolution, the relative position of the highest peak with respect to $(I_2, J_2 - 10)$ in PLRV will be the same as the relative position of REFV (1, 1) with respect to $(I_1, J_1 - 10)$ in PHRV. Therefore, the highest peak is expected at

$$[I_2 - (I_1 - K_2), J_2 - 10 - (J_1 - 10 - L_2)]$$
$$= [I_2 - (I_1 - K_2), J_2 - (J_1 - L_2)] \quad (7)$$

For the Scene 3,

$$I_1 = 34, J_1 = 21$$
$$I_2 = 39, J_2 = 34 \quad (8)$$
$$K_2 = 18, L_2 = 13$$

Substituting 8 into 7 reveals that the peak should appear at [23, 26]. This is clearly shown in Figure 4.

EED28.CORJ3B32 is the correlation surface of size 41 x 36 obtained by correlating the 32 x 32 REFV from PHRV with PHRV itself. Therefore the peak will appear at (K_2, L_2) and its value will be 1024 since auto-correlation yields perfect registration at the peak. Since this correlation surface is used to generate EED28.CORJ3C32 and has no other significance, the results of EED28.CORJ3B32 are not tabulated. However, this correlation surface, its peak and PHRV are shown in Figure 5a.

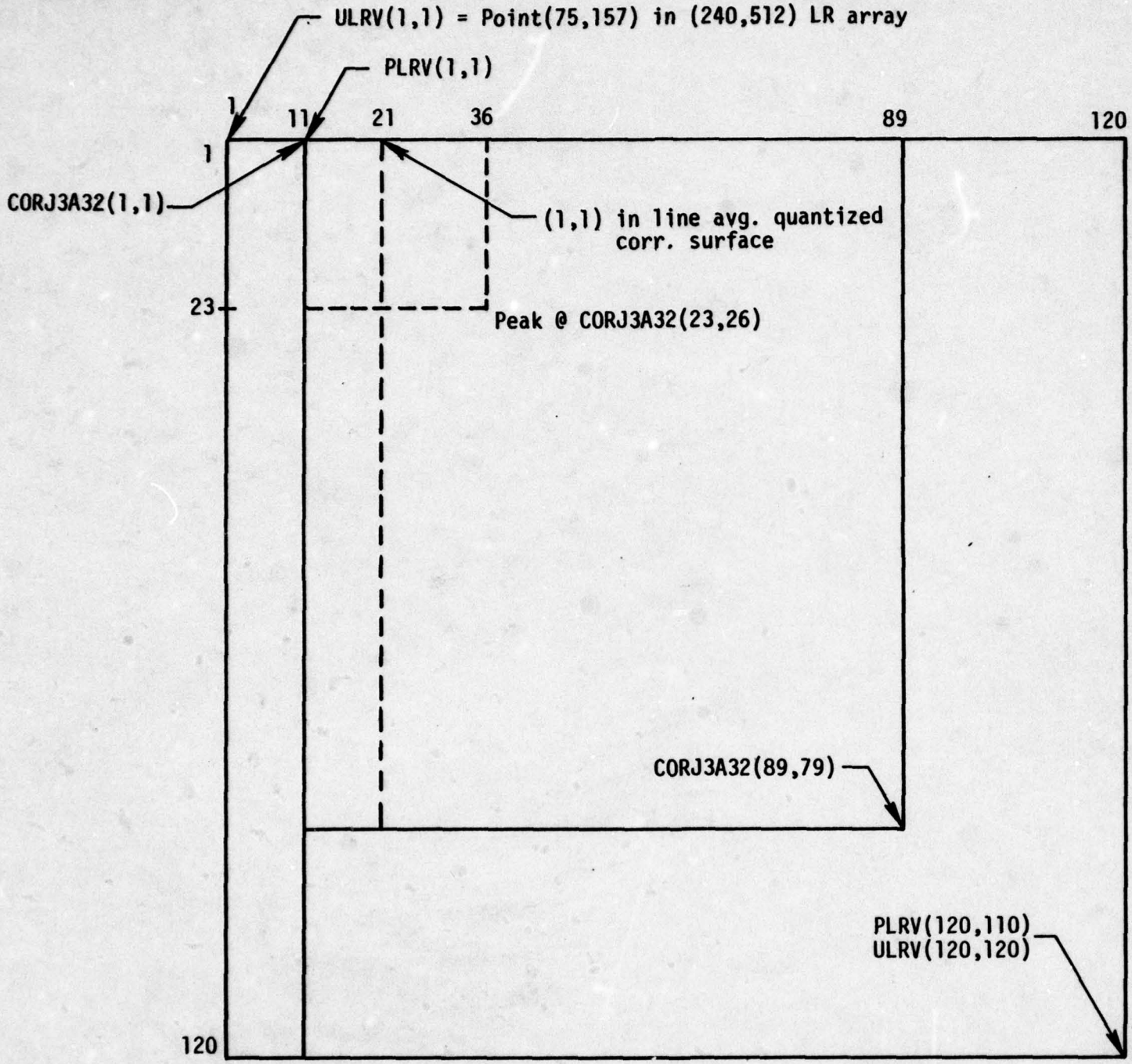

Figure 4. Correlation peak in CORJ3A32.

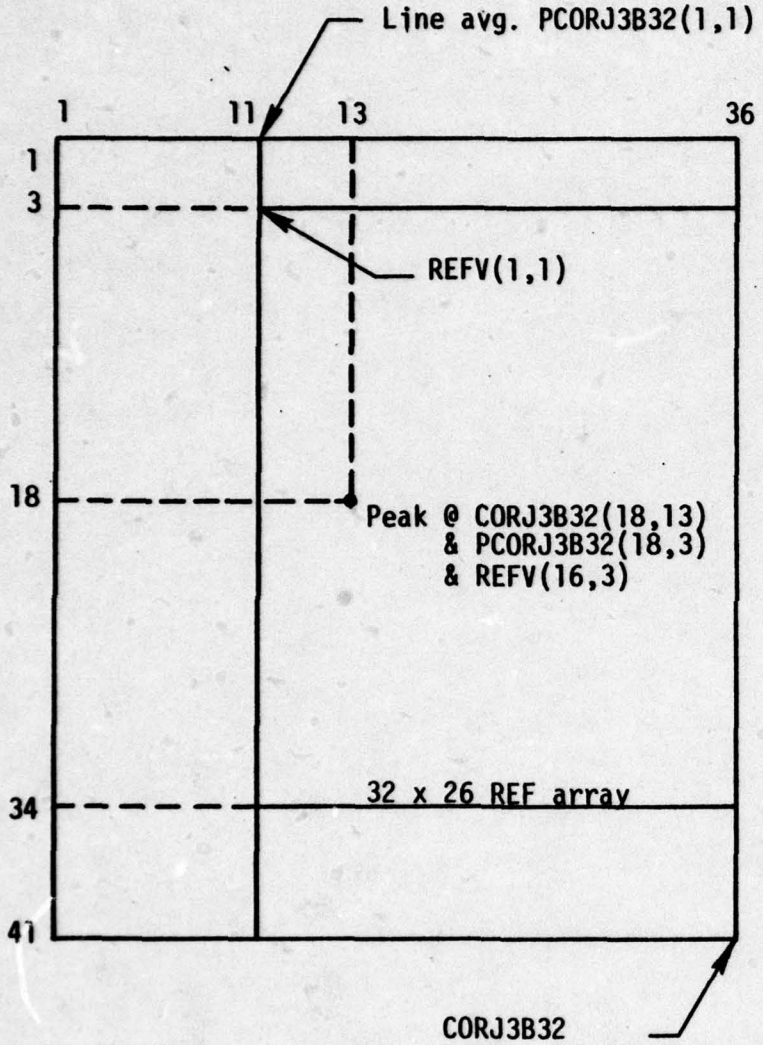

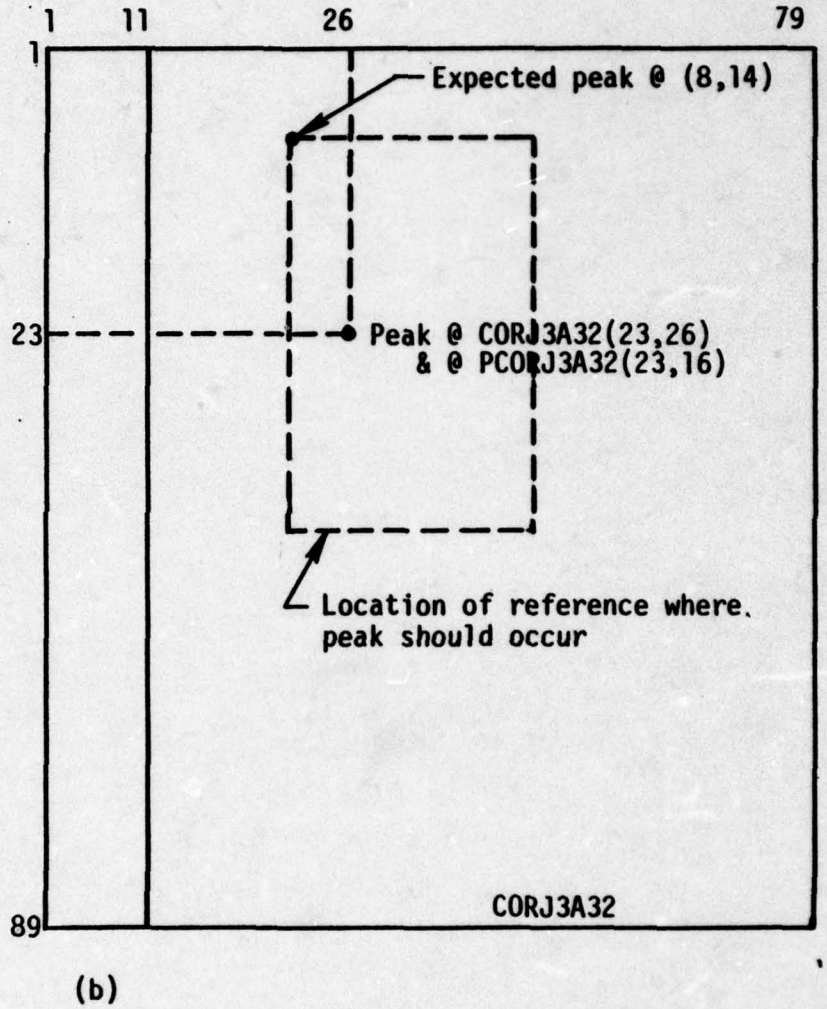

Figure 5. Arrays and expected peak in (32 x 32) autocorrelation.

EED28.CORJ3C32 is the correlation surface obtained by correlating the autocorrelation surface EED28.CORJ3B32 with EED28.CORJ3A32. Basically the approach is the same as discussed before. The REFV chosen from the processed CORJ3B32 array is centered about the peak in the correlation surface. Since the array CORJ3B32 contains only 26 columns after line average quantization, a REFV of size 32 x 26 is chosen as shown in Figure 5a. Figure 5b shows the location of the REFV in the processed CORJ3A32 array and the coordinates of the expected peak in the correlation surface EED28.CORJ3C32.

The same result can be achieved by calculation as follows. The relative position of the expected peak in EED28.CORJ3C32 with respect to the peak at (23, 25) in PCORJ3A32 should be the same as that of REFV (1, 1) with respect to (18, 3) in the processed CORJ3B32 array. Therefore the peak in EED28.CORJ3C32 is expected at

$$[23 - (18 - 3),\ 16 - (3 - 1)] = [8, 14]$$

The results of this simulation are given in Table 1 at end of chapter.

Figures 6 - 8 illustrate the generation of EED28.CORJ3A16, EED28.CORJ3B16 and EED28.CORJ3C16 using a reference array of size 16 x 16. The results of simulation are tabulated in Table 2.

B. Correlation Using Analog Preprocessing Filter as Quantizer

The transfer function G(s) of the analog preprocessing filter is given by Equation 9.

$$G(s) = \frac{2.21\, W_2\, S^2}{(S + W_1)(S + W_2)(S + W_3)} \qquad (9)$$

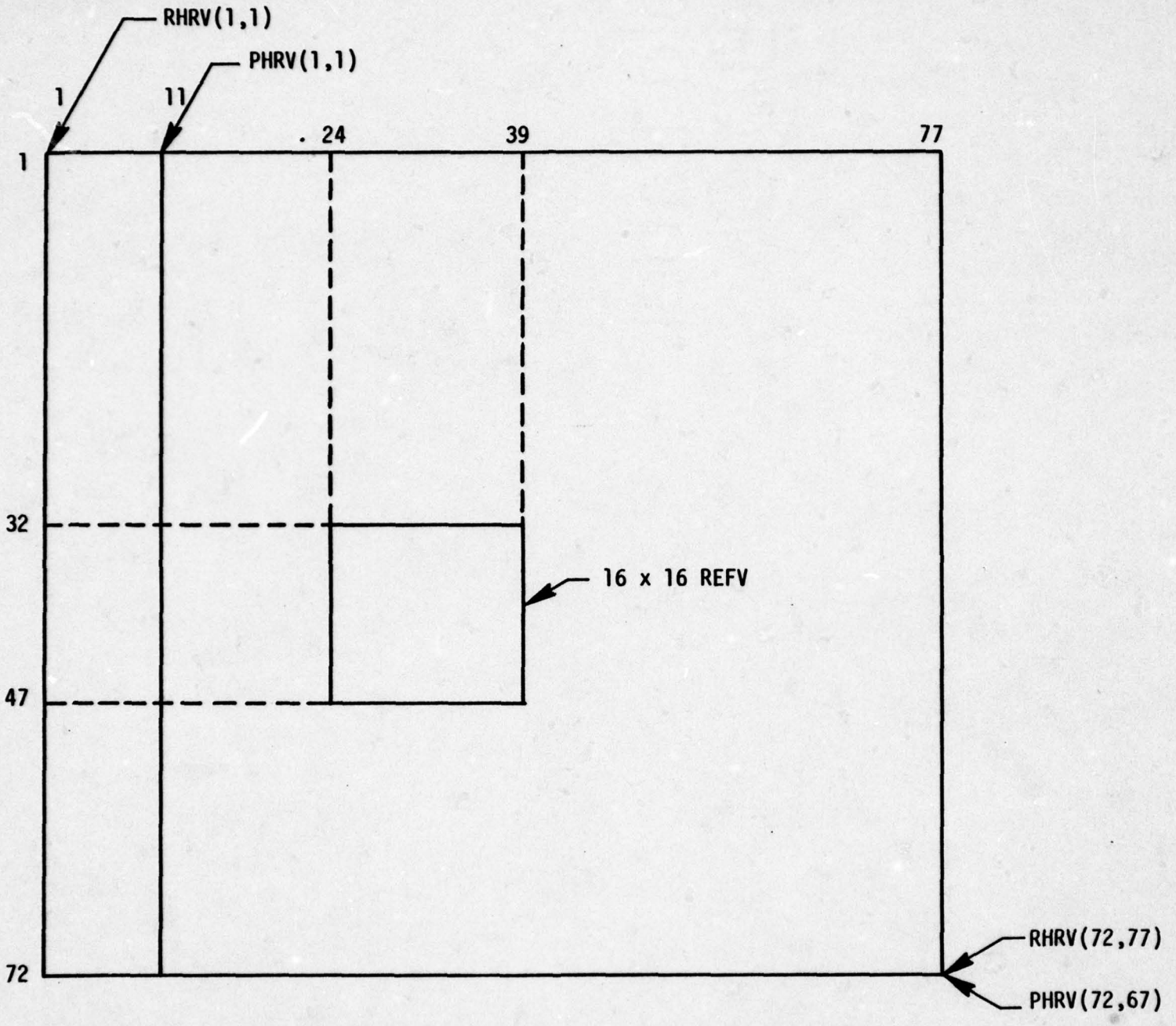

Figure 6. 16 x 16 reference array in processed high resolution video.

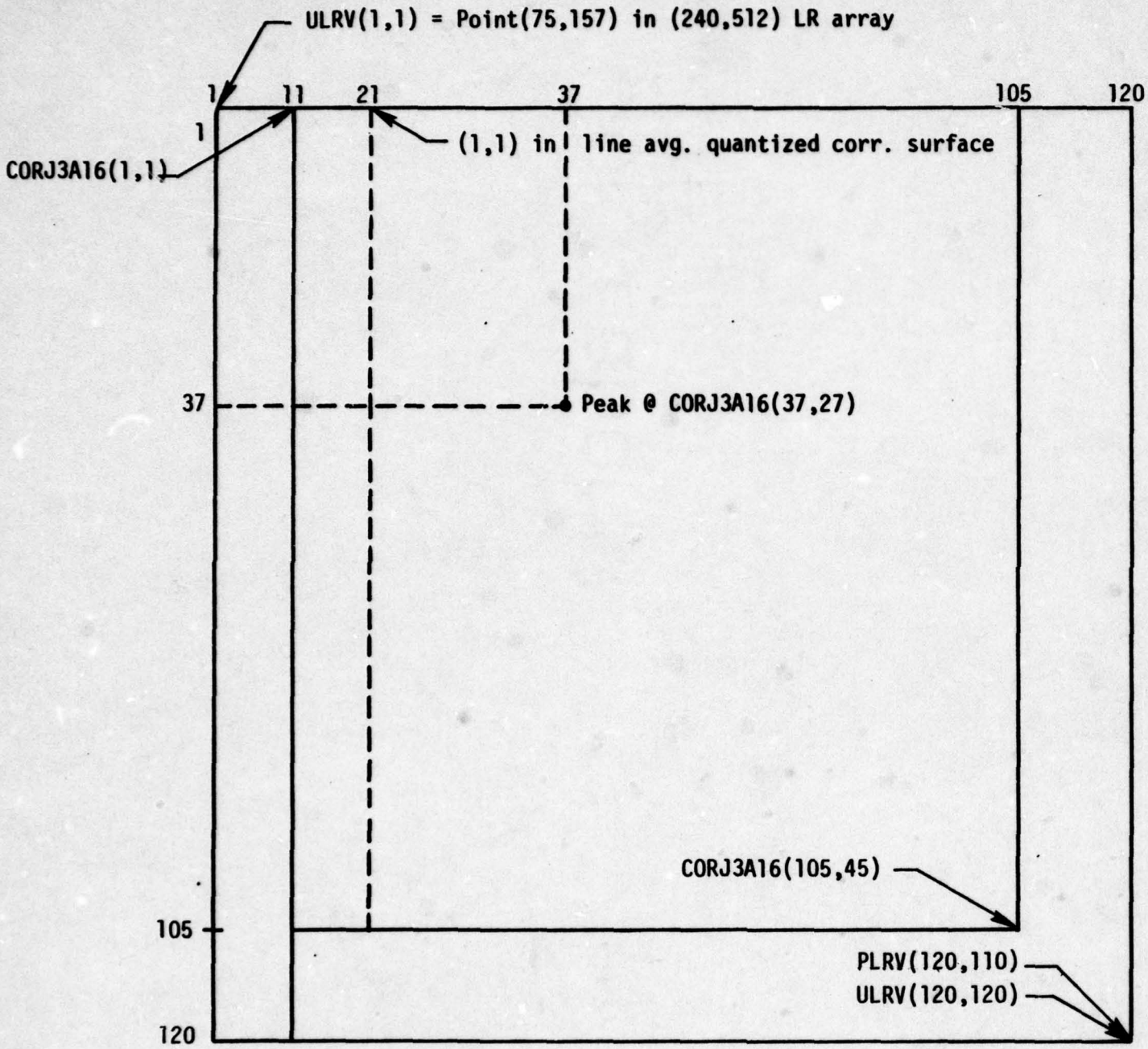

Figure 7. Expected correlation peak in CORJ3A16 array.

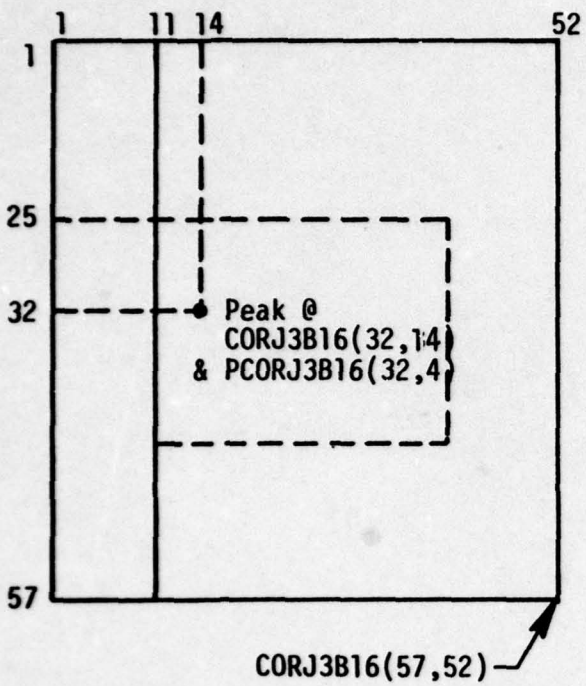

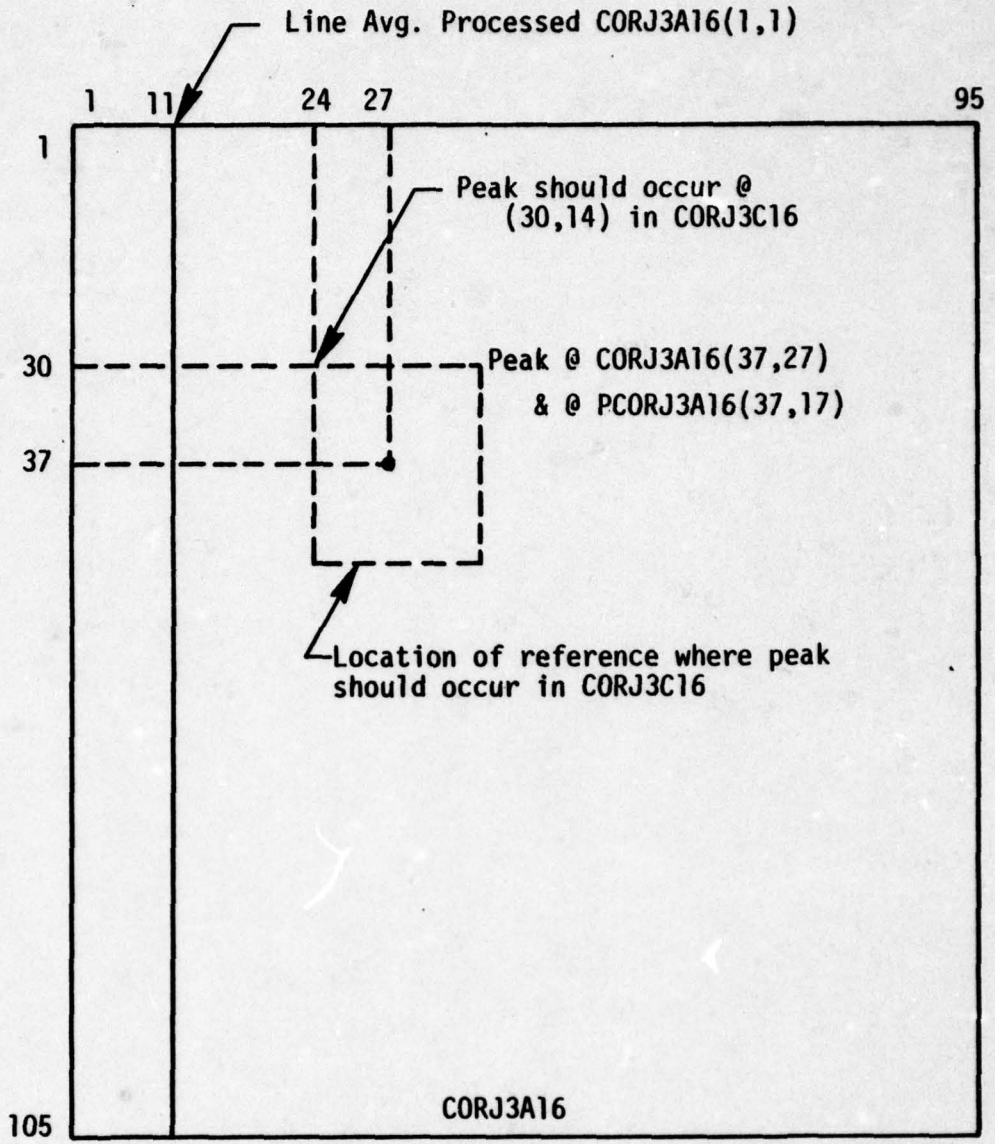

Figure 8. 16 x 16 autocorrelation arrays and expected peaks.

This filter has zero dc gain and therefore transforms the input video to zero mean video. In order to process a digital image, the analog filter is transformed to a digital filter by bilinear transformation as explained below.

In bilinear transformation, the digital transfer function H(z) is obtained from analog transfer function G(s) by the substitution

$$S = \frac{2}{T} \cdot \frac{Z-1}{Z+1}$$

That is

$$H(Z) = G(s)\Big|_{S = \frac{2}{T} \cdot \frac{Z-1}{Z+1}} \tag{10}$$

where T = sampling period.

The price paid for this is the introduction of a distortion in the frequency axis.

Equation 10 can be used if the distortion can be tolerated, which is generally true if the sampling frequency is very high compared to the critical frequencies (W_1, W_2 and W_3). Otherwise, if the critical frequencies of the analog filter are prewarped as shown by Equations 10a, 10b, 10c, then, when the analog filter is transformed to a digital filter using Equation 10d, the digital filter will meet the desired specifications.

$$W_1' = \tan\left(\frac{W_1 T}{2}\right) \tag{10a}$$

$$W_2' = \tan\left(\frac{W_2 T}{2}\right) \tag{10b}$$

$$W_3' = \tan\left(\frac{W_3 T}{2}\right) \tag{10c}$$

$$H(Z) = G'(s)\Big|_{S = \frac{Z-1}{Z+1}} \tag{10d}$$

Therefore, G(s) in Equation 9 can be written as

$$G(s) = \frac{2.21\, W_2' s^2}{s^3 + (W_1' + W_2' + W_3')s^2 + (W_1'W_2' + W_2'W_3' + W_3'W_1')s + W_1'W_2'W_3'} \tag{11}$$

From Equation 10d,

$$H(Z) = \frac{2.21\, W_2' \left(\frac{Z-1}{Z+1}\right)^2}{\left(\frac{Z-1}{Z+1}\right)^3 + (W_1' + W_2' + W_3')\left(\frac{Z-1}{Z+1}\right)^2 + (W_1'W_2' + W_2'W_3' + W_3'W_1')\left(\frac{Z-1}{Z+1}\right) + W_1'W_2'W_3'} \tag{12}$$

Letting

$$\begin{aligned} A &= (W_1' + W_2' + W_3') \\ B &= (W_1'W_2' + W_2'W_3' + W_3'W_1') \\ C &= W_1'W_2'W_3' \\ D &= 2.21\, W_2' \end{aligned} \tag{13}$$

one obtains

$$H(Z) = \frac{D\left(\frac{Z-1}{Z+1}\right)^2}{\left(\frac{Z-1}{Z+1}\right)^3 + A\left(\frac{Z-1}{Z+1}\right)^2 + B\left(\frac{Z-1}{Z+1}\right) + C} \tag{14}$$

Simplifying the above equation yields

$$H(Z) = \frac{a(Z^3 - Z^2 - Z + 1)}{b_1 Z^3 + b_2 Z^2 + b_3 Z + 1} \tag{15}$$

where,

$$\begin{aligned} a &= D/(A - B + C - 1) \\ b_1 &= (A + B + C + 1)/(A - B + C - 1) \\ b_2 &= (-A + B + 3C - 3)/(A - B + C - 1) \\ b_3 &= (-A - B + 3C + 3)/(A - B + C - 1) \end{aligned} \tag{16}$$

But $$H(Z) = \frac{Y(Z)}{X(Z)} \tag{17}$$

where, $Y(Z)$ is the Z-transform of the output sequence $\{Y(n)\}$ and

$X(Z)$ is the Z-transform of the input sequence $\{X(n)\}$

From Equations 15 through 17,

$$\frac{Y(Z)}{X(Z)} = \frac{a(Z^3 - Z^2 - Z + 1)}{b_1Z^3 + b_2Z^2 + b_3Z + 1} \tag{18}$$

Cross multiplying both sides of Equation 18 yields

$$(b_1Z^3 + b_2Z^2 + b_3Z + 1)Y(Z) = a(Z^3 - Z^2 - Z + 1)X(Z) \tag{19}$$

Taking the inverse Z-transform of Equation 19 yields

$$\begin{aligned} y(n) = {} & a[x(n) - x(n-1) - x(n-2) + x(n-3)]/b_1 \\ & -[b_2\, y(n-1) + b_3\, y(n-2) + y(n-3)]/b_1 \end{aligned} \tag{20}$$

Equation 20, where the constants are described by Equation 16, describing the digitized analog preprocessing filter and can be easily simulated on digital computers.

1. Quantization of RHRV

The coefficients a, b_1, b_2 and b_3 of the difference equation described by Equation 16 are computed, assuming

$$\begin{aligned} W_1 &= 984\pi \\ W_2 &= 1100278\pi \\ W_3 &= 58062\pi \\ T &= 0.2 \times 10^{-6} \text{ sec.} \end{aligned} \tag{21}$$

NR = Number of rows in RHRV

NC = Number of columns in RHRV

An input sequence $\{x(\eta)\}$ of length NR · NC is formed by joining the successive rows of RHRV. The first three elements of the output sequence $\{y(\eta)\}$ are initialized to zero. Then, all other elements of $\{y(\eta)\}$ are computed using Equation 20. The first NC elements of the output sequence $\{y(\eta)\}$ form the first row of the zero mean video (ZMV), and the second NC elements of $\{y(\eta)\}$ form the second row of ZMV, etc. Equation 22 describes the quantization process of the zero mean video to obtain PHRV, the binary form of RHRV.

$$PHRV(I,J) = \begin{cases} 1 & , \text{ If } ZMV(I,J) \geq DELTA \\ 0 & , \text{ If } ZMV(I,J) < DELTA \end{cases} \qquad (22)$$

where, DELTA is the quantization threshold which yields approximately an equal number of zeros and ones in REFV. Its value is determined by simulation.

The method of choosing the reference array from RHRV was discussed in a previous section. For Scene 3, RHRV, PHRV and reference arrays of size 32 x 32, 16 x 16 and 8 x 8 are shown in Figure 9.

2. Quantization of ULRV

The quantization process of ULRV is identical to that of RHRV with the following two changes.

a. The coefficients a, b_1, b_2 and b_3 are computed, assuming

$$W_1 = 984\pi$$

$$W_2 = 1100278\pi \qquad (23)$$

$$W_3 = 174052\pi$$

and $T = 0.2 \times 10^{-6}$ sec.

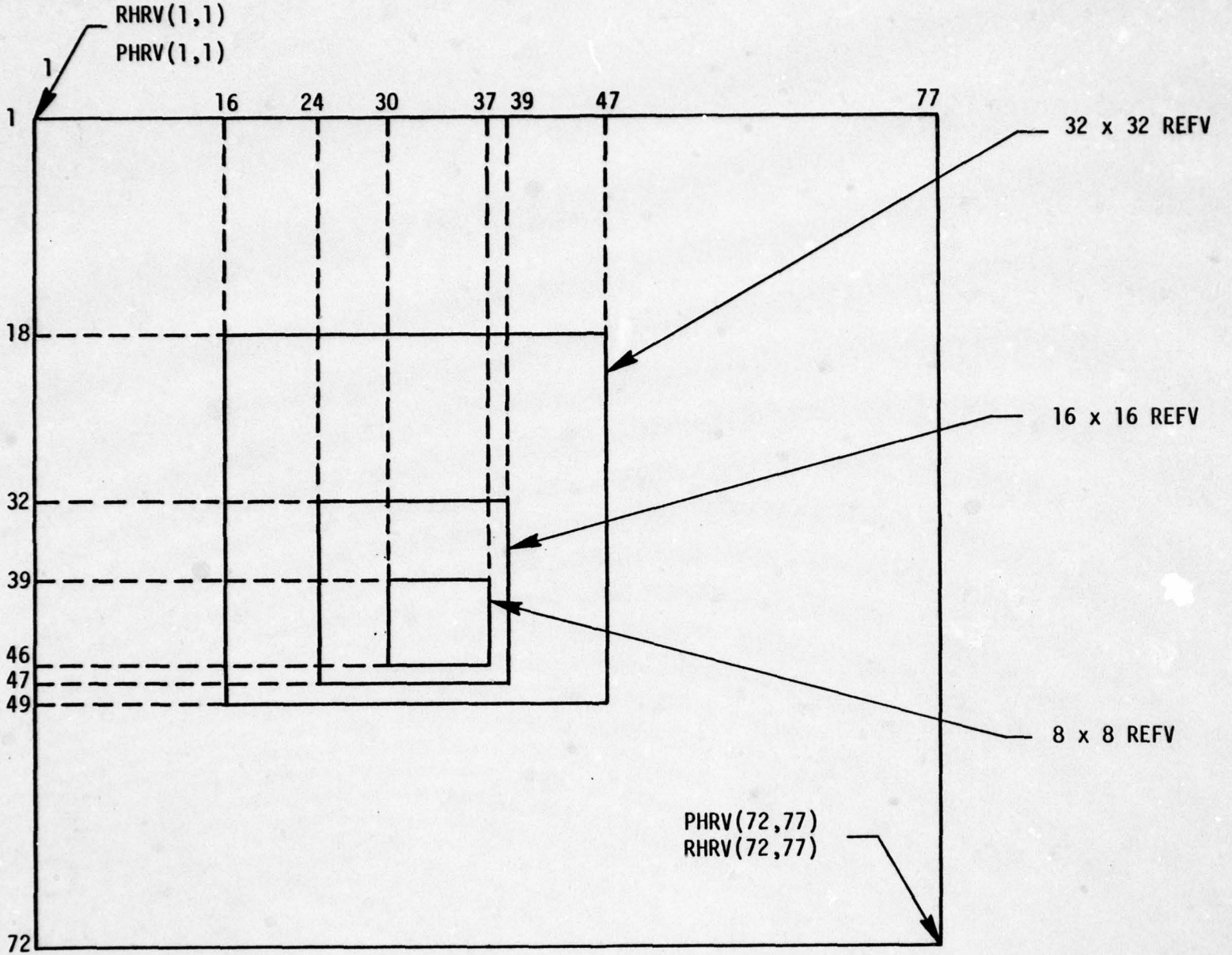

Figure 9. 8 x 8, 16 x 16 and 32 x 32 reference arrays in RHRV and PHRV.

b. The quantization process of zero mean video to obtain PLRV, the binary form of ULRV, is modified as in Equation 24.

$$PLRV(I,J) = \begin{cases} 1 & , \text{ If } ZMV(I,J) \geq 0 \\ 0 & , \text{ If } ZMV(I,J) < 0 \end{cases} \quad (24)$$

3. Correlation Array's EED28.CORJ3D32, EED28.CORJ3E32 and EED28.CORJ3F32

EED28.CORJ3D32 is the correlation array of size 89 x 89 obtained by correlating a REFV of size 32 x 32 with PLRV of size 120 x 120. The first four highest peaks and their coordinates are tabulated in Table 1. The average value of the correlation surface excluding the 7 x 7 array centered at the peak, the standard deviation of the correlation surface excluding the 7 x 7 array centered at the peak and the signal-to-noise ratio are also computed.

The methods of calculating the coordinates of the expected peak is similar to that discussed in Section A and the expected peak is shown in Figure 10. EED28.CORJ3E32 is the correlation surface of size 41 x 46 obtained by correlating a 32 x 32 REFV with PHRV. This correlation surface and its peak in PHRV are shown in Figure 11(a).

EED28.CORJ3F32 is the correlation surface obtained by correlating the correlation surface EED28.CORJ3D32 with the reference array from the correlation surface EED28.CORJ3E32. The method of choosing the REFV from EED28.CORJ3E32 is the same as that discussed in Section A and is clearly indicated in Figures 11(a) and 11(b). Figures 12 and 13 illustrate the generation of EED28.CORJ3D16, EED28.CORJ3E16 and EED28.CORJ3F16. Simulation results are tabulated in Table 2.

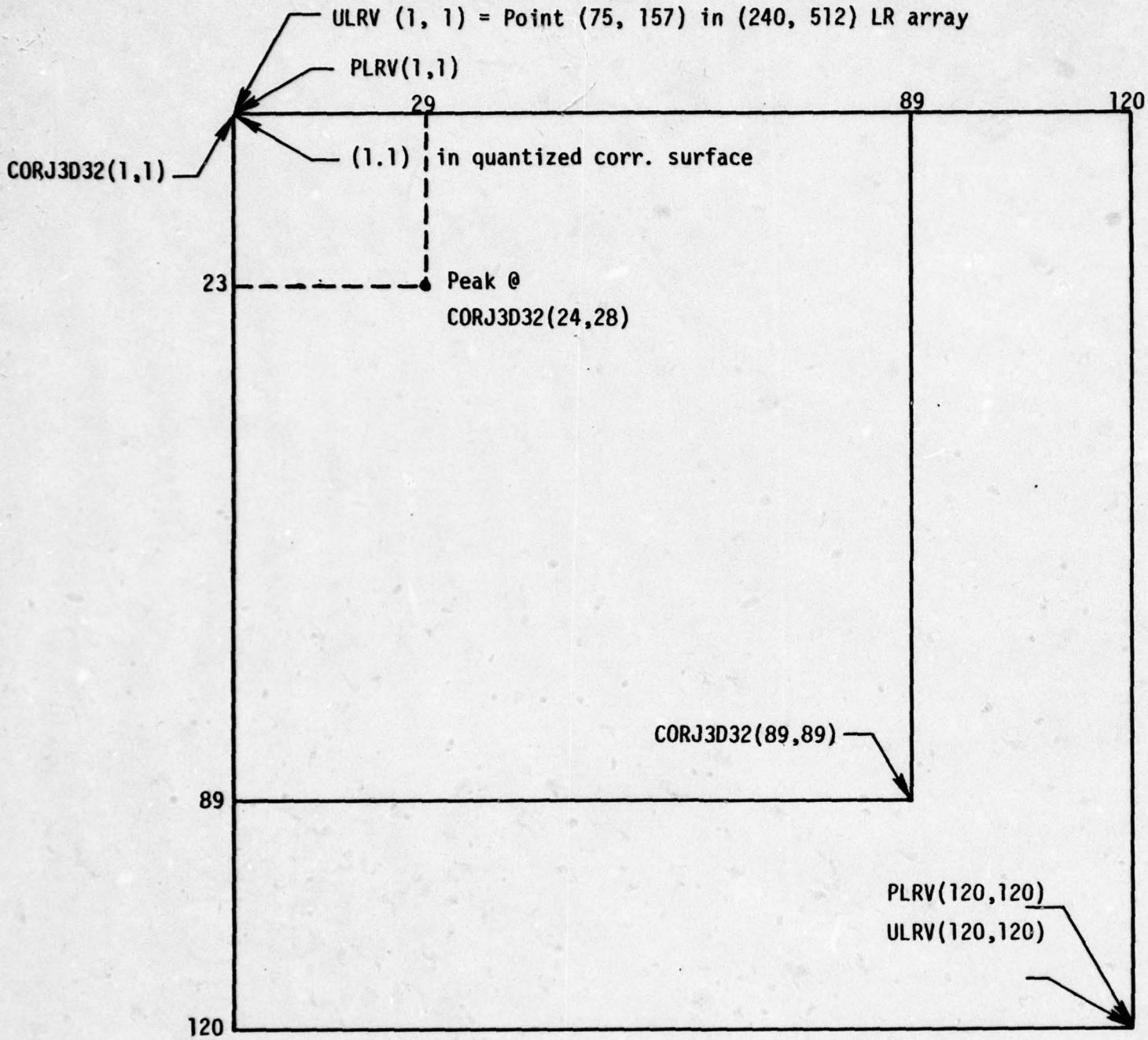

Figure 10. Expected peak in CORJ3D32 array.

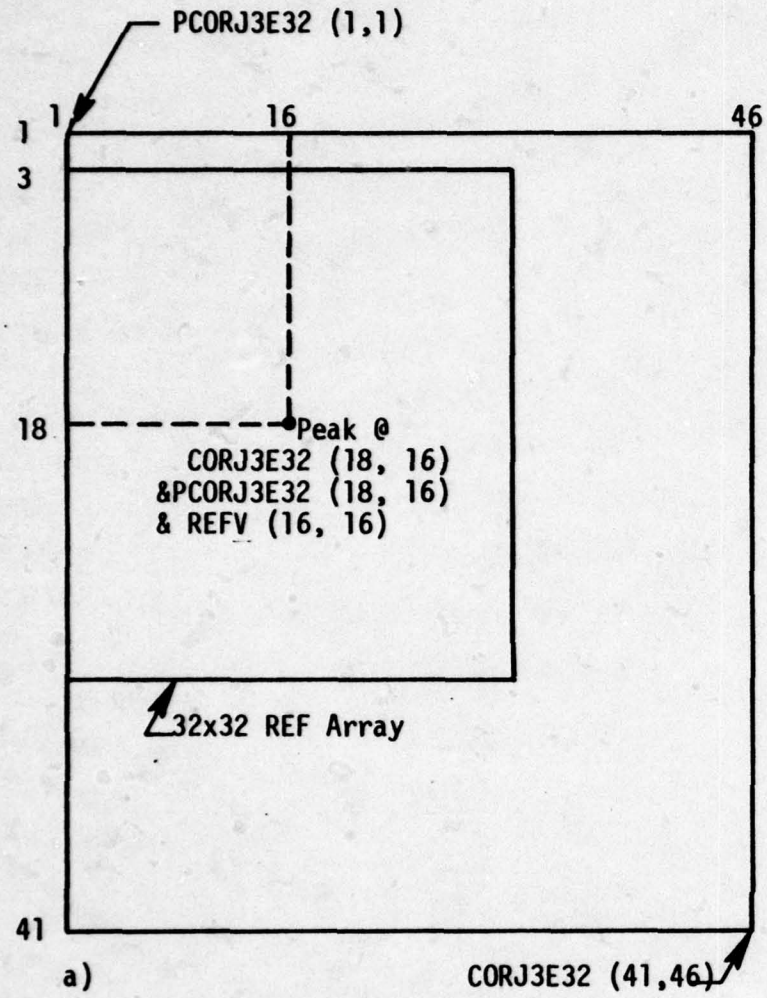

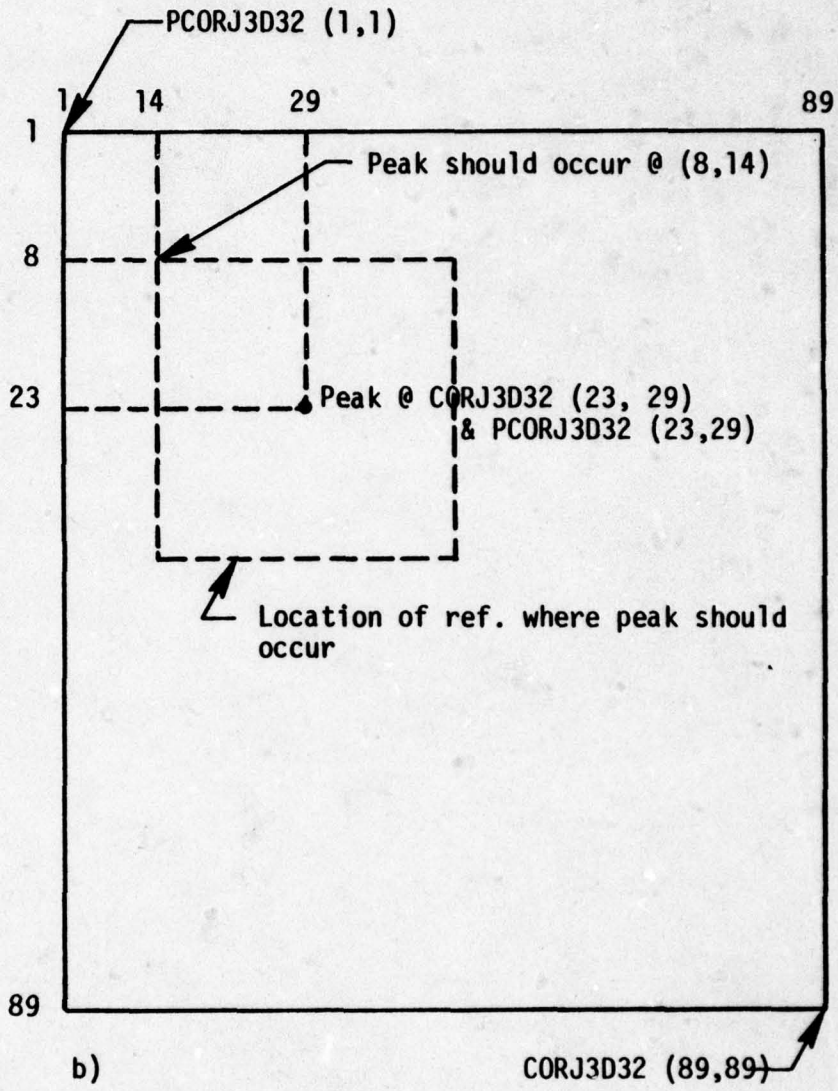

Figure 11. 32 x 32 autocorrelation arrays and expected peaks.

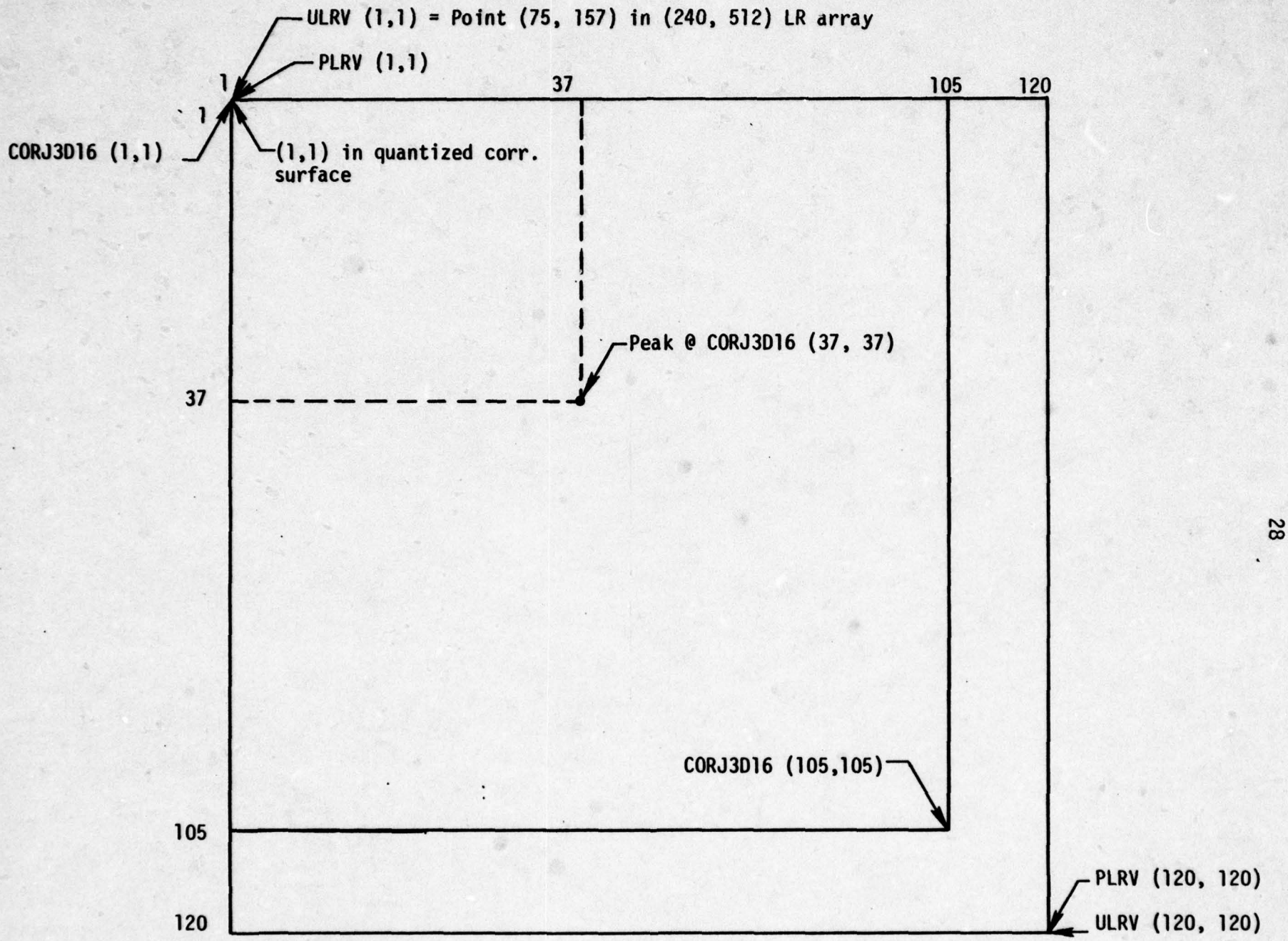

Figure 12. Expected correlation peak in CORJ3D16 array.

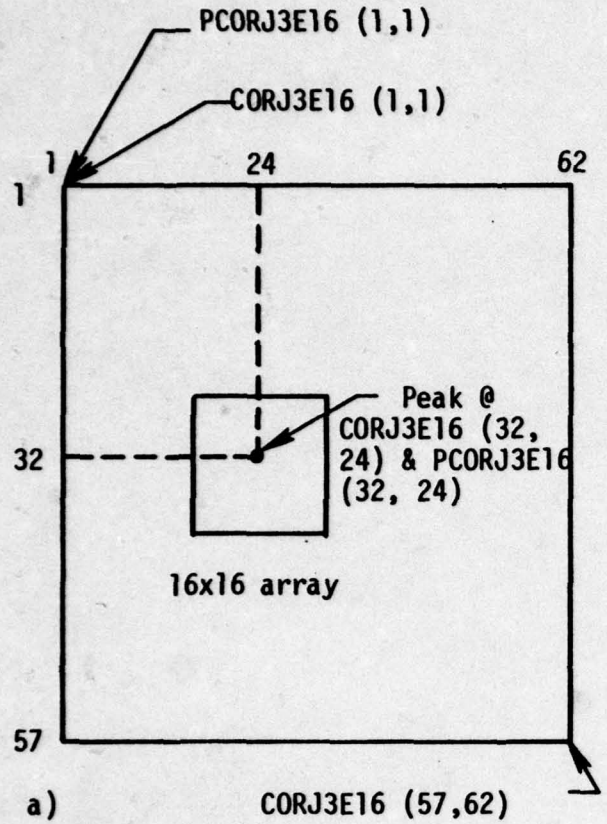

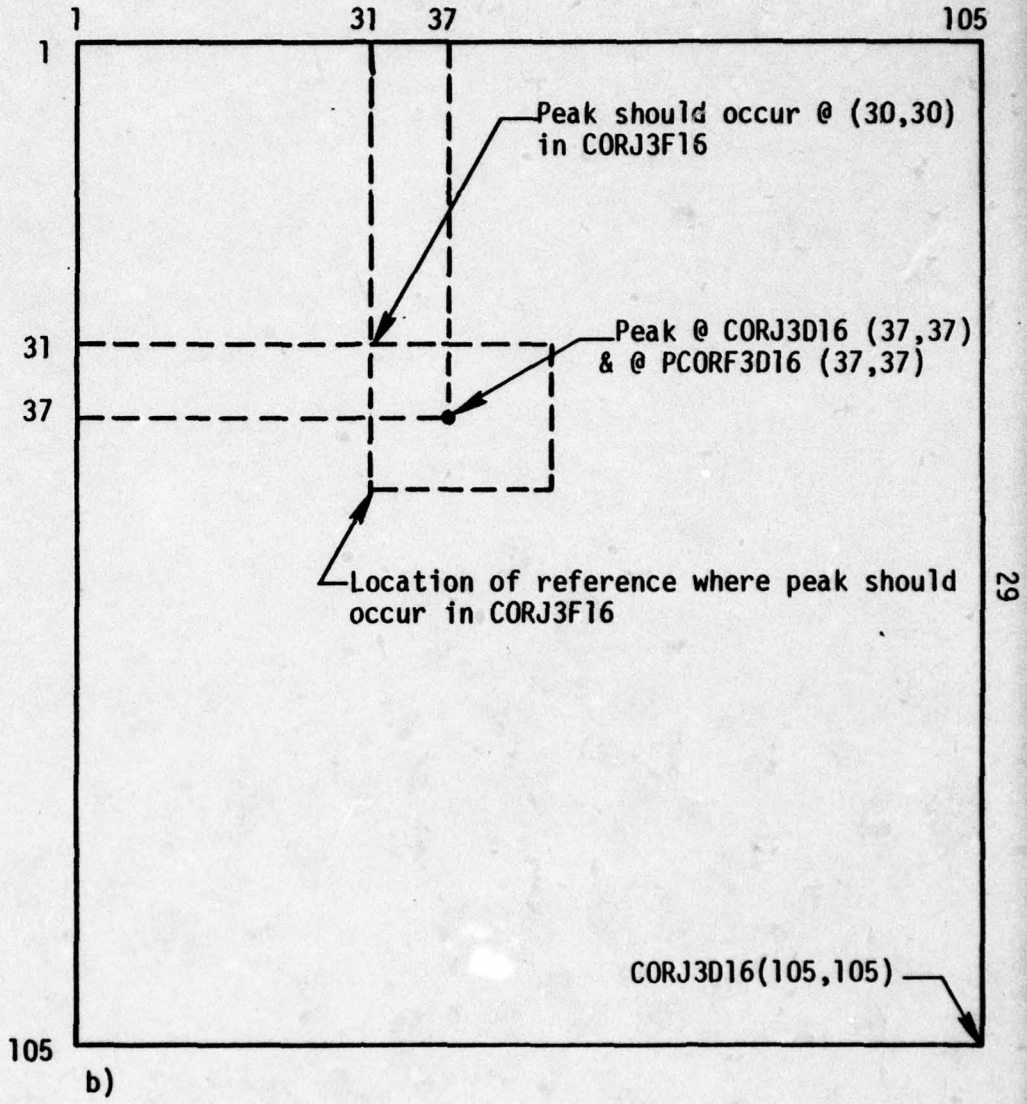

Figure 13. 16x16 autocorrelation arrays and expected peaks.

C. Correlation Using Array Average Quantizer

Consider the layout of the input video array as given in Figure 14. The pixel to be quantized is located in the center of a K x L subarray of pixel values. The average value used for the threshold is based on the average value of the K x L pixel subarray. Equation (25) details the average value calculation.

$$\bar{X}(i, j) = \frac{1}{KL} \sum_{I=1}^{K} \sum_{J=1}^{L} X(i - k - 1 + I, j - \ell - 1 + J) \quad (25)$$

where k = largest integer $\leq K/2$

ℓ = largest integer $\leq L/2$

Equation (26) gives the quantization process

$$X_q(i, j) = \begin{cases} 1 & ; \ X(i, j) \geq \bar{X}(i, j) \\ 0 & ; \ X(i, j) < \bar{X}(i, j) \end{cases} \quad (26)$$

Because there is a border region of the input array which will be quantized incorrectly, the resulting quantized array has $(N - K + 1) \times (M - L + 1)$ pixels. The rest of the procedure is similar to that using the line average quantizer. EED28.CORJ3G32 is the correlation array of size 79 x 79 obtained by correlating REFV of size 32 x 32 with PLRV of size 110 x 110.

EED28.CORJ3H32 is the correlation surface obtained by correlating the 32 x 32 REFV from PHRV with PHRV itself. EED28.CORJ3I32 is the correlation surface obtained by correlating the correlation surface EED28.CORJ3G32 with EED28.CORJ3H32. A similar analysis is done for a reference array of size 16 x 16. Details are clearly shown in Figures 15 - 19.

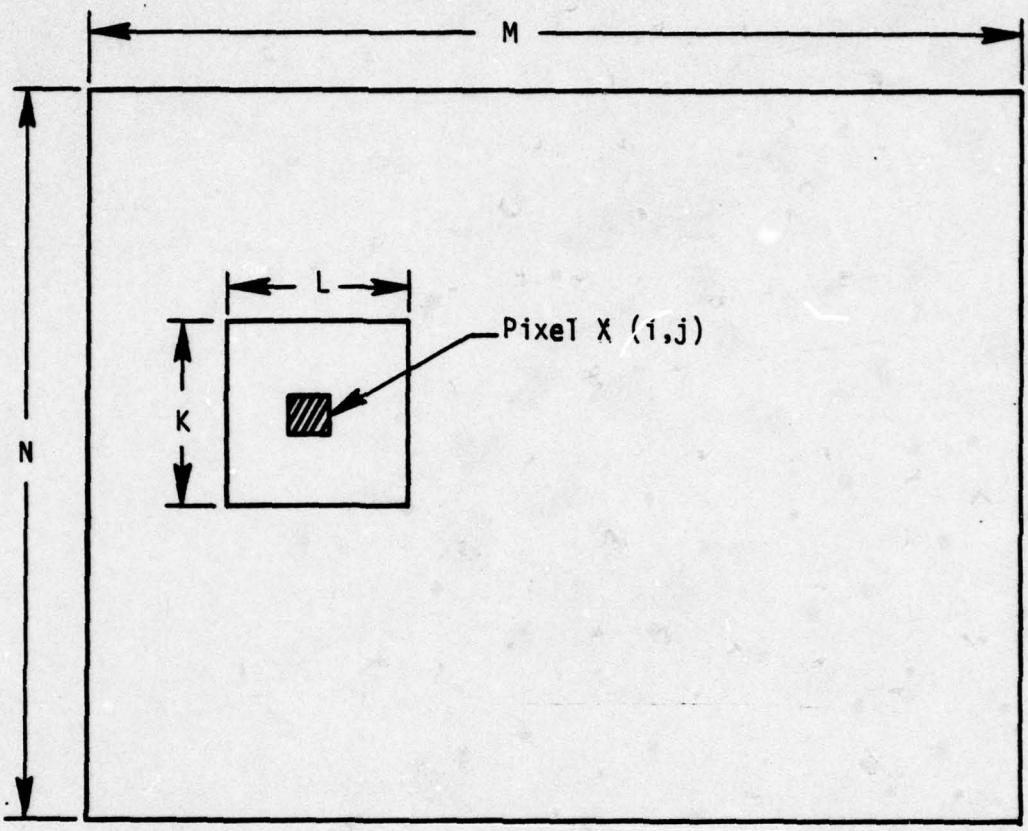

Figure 14. Layout of the input array for quantization based on an array quantizer.

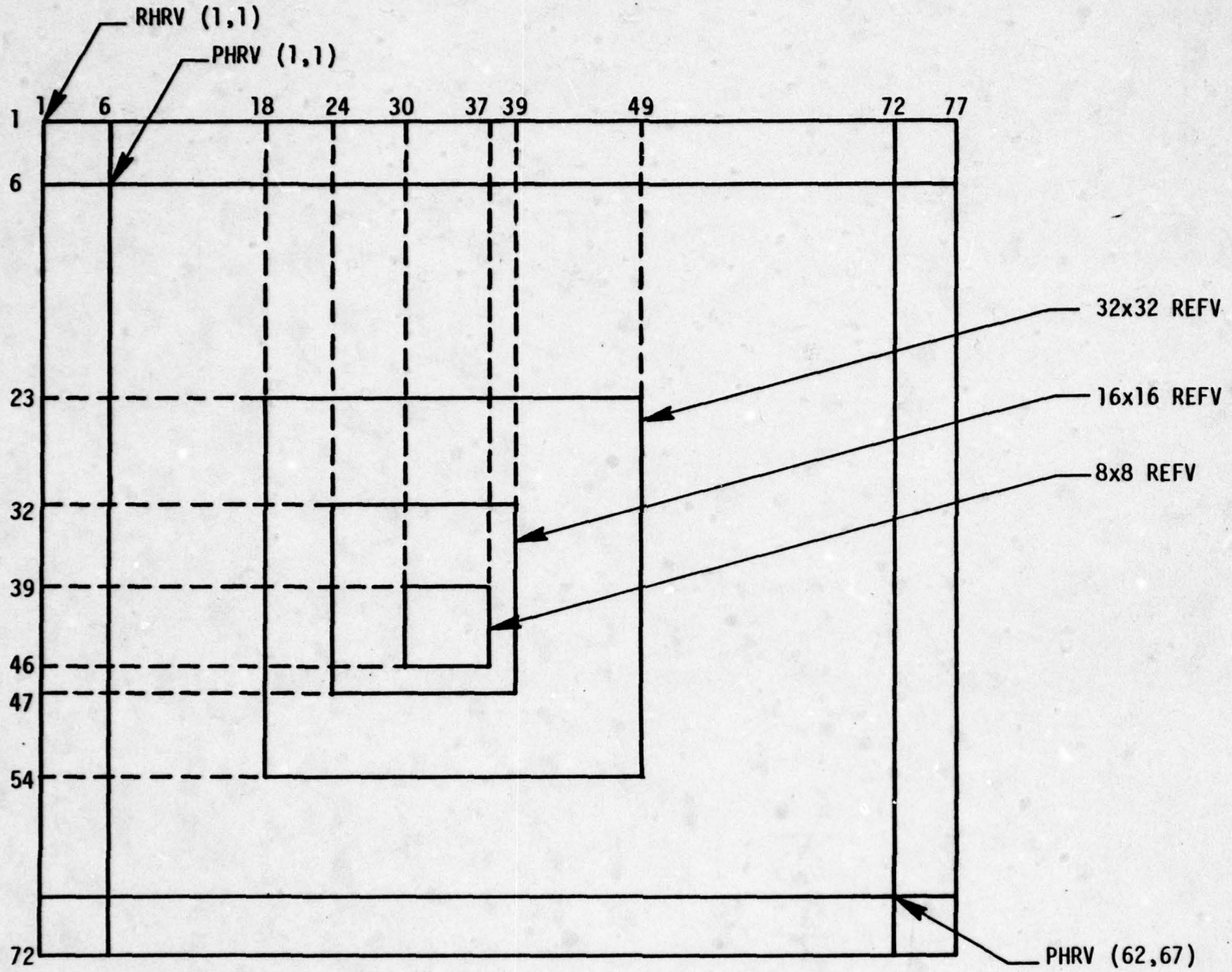

Figure 15. 8x8, 16x16 and 32x32 reference arrays in RHRV and PHRV.

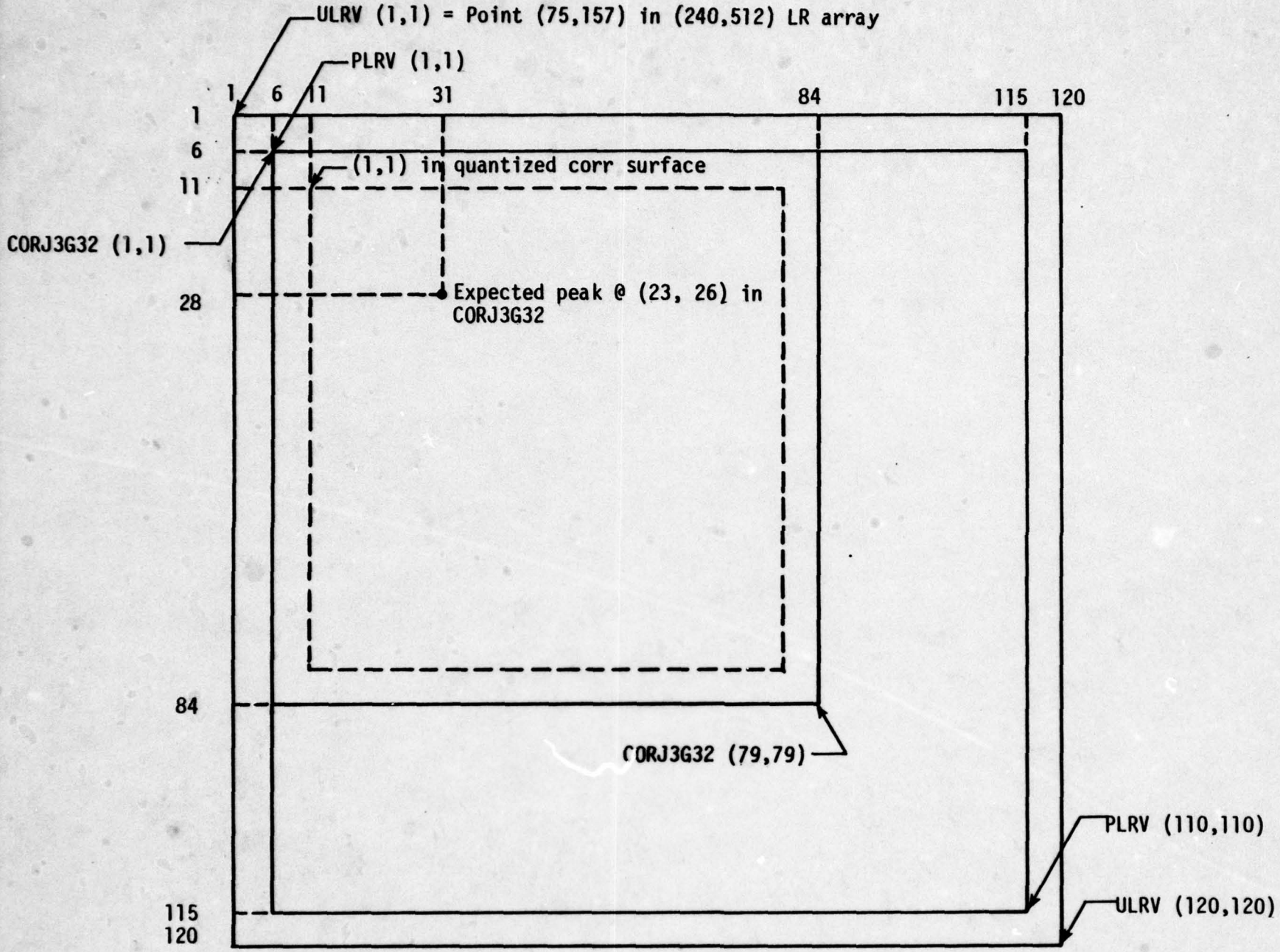

Figure 16. Expected peak in CORJ3G32 array.

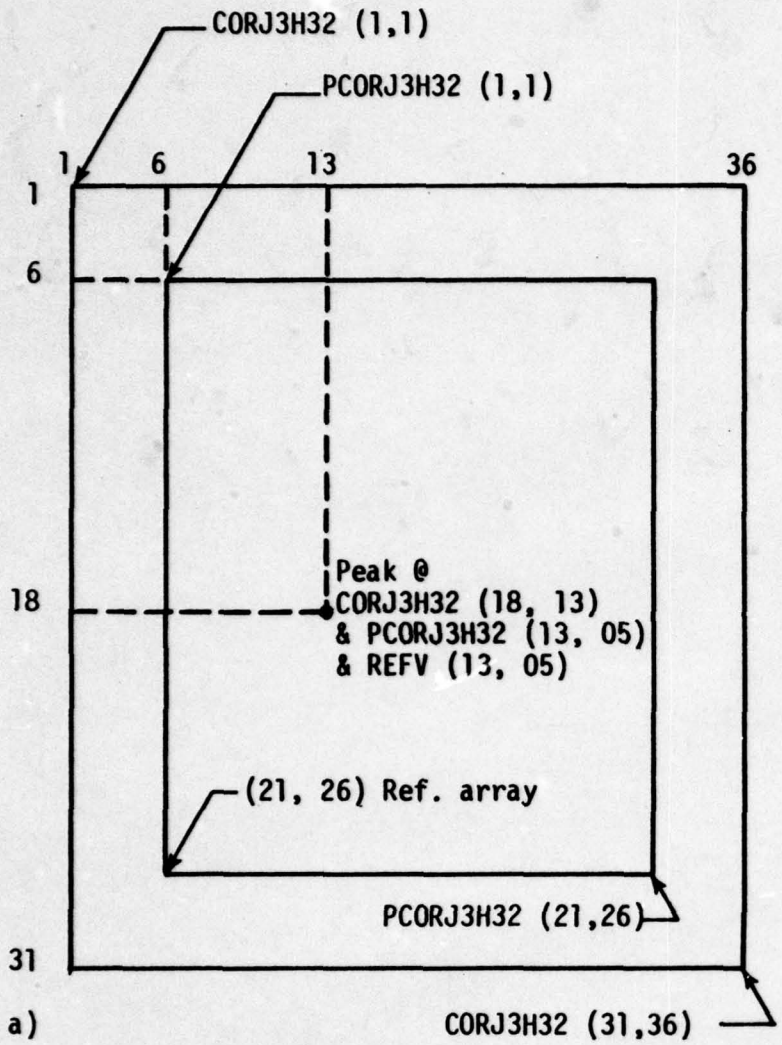

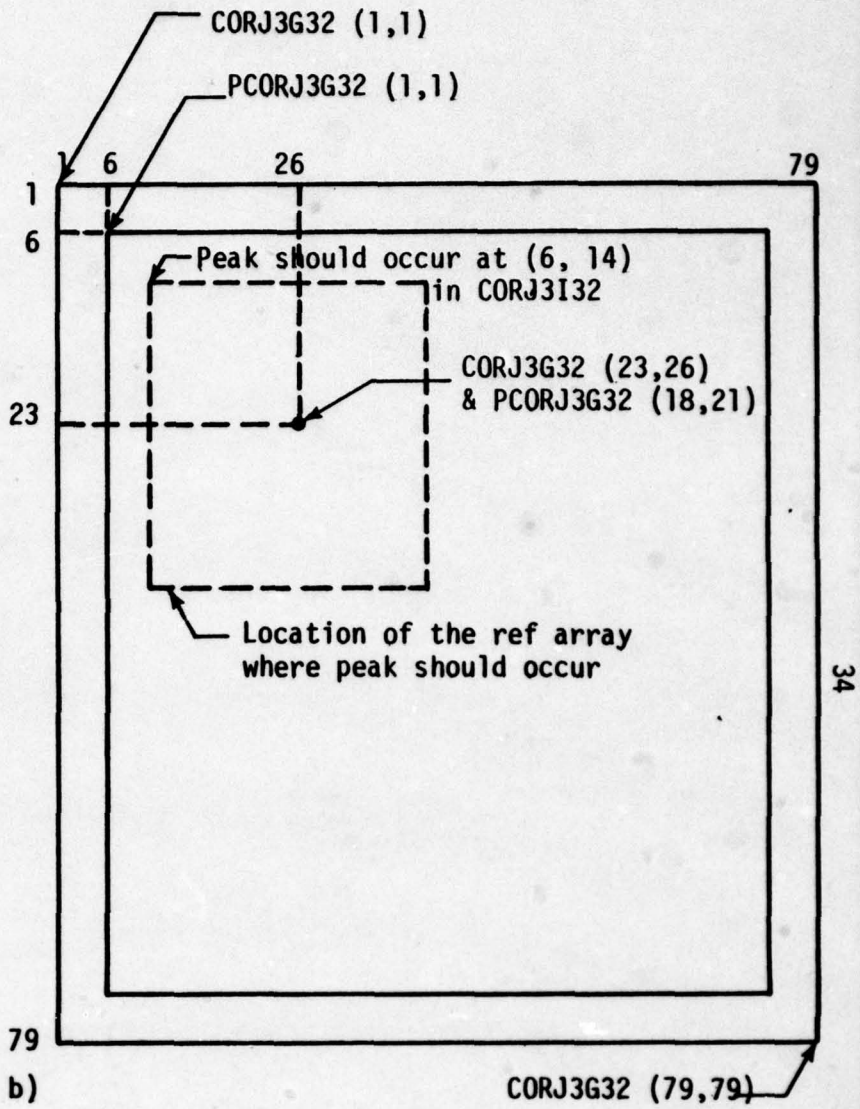

Figure 17. 32x32 autocorrelation array and expected peaks.

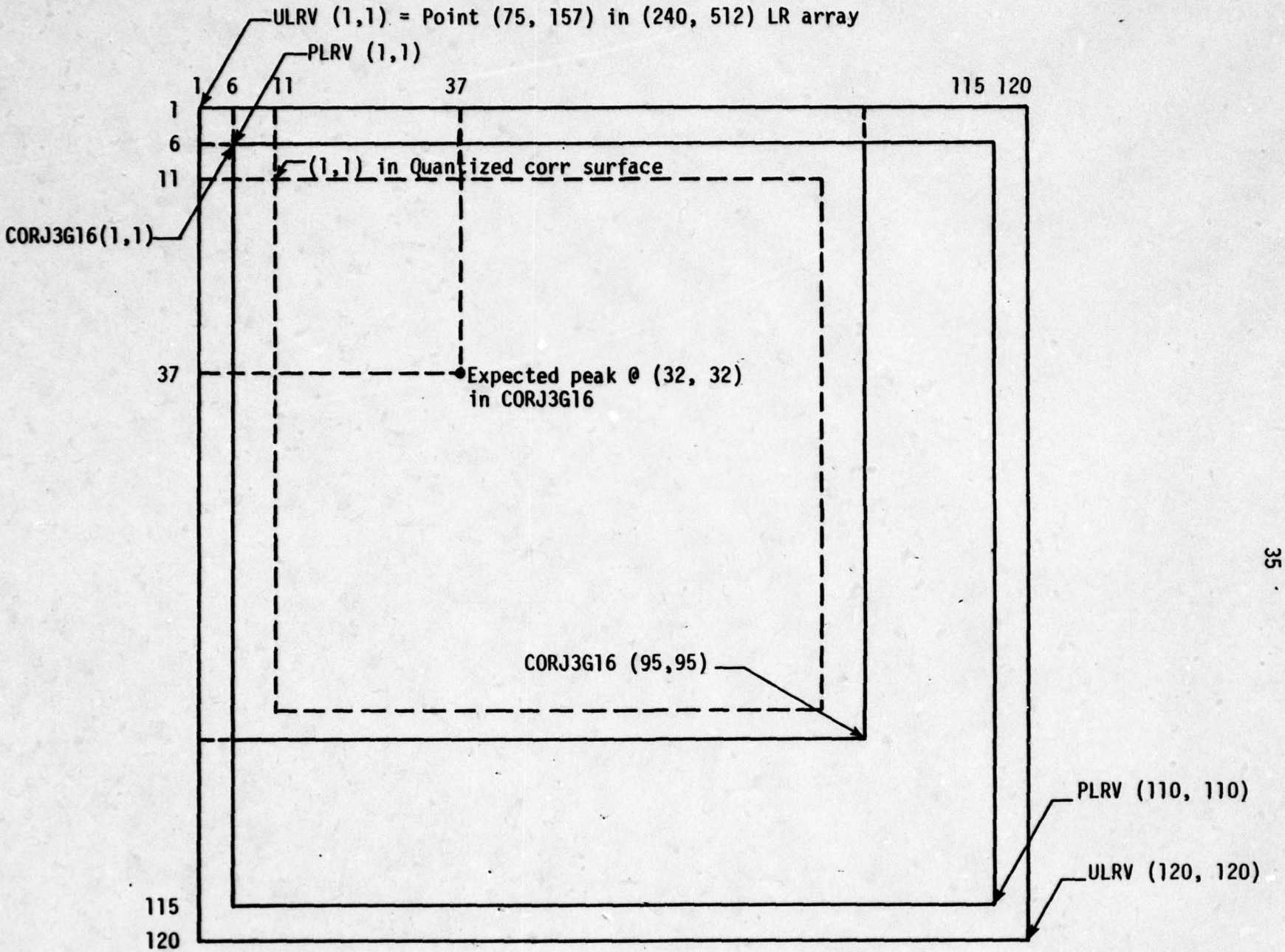

Figure 18. Expected peak in CORJ3G16 array.

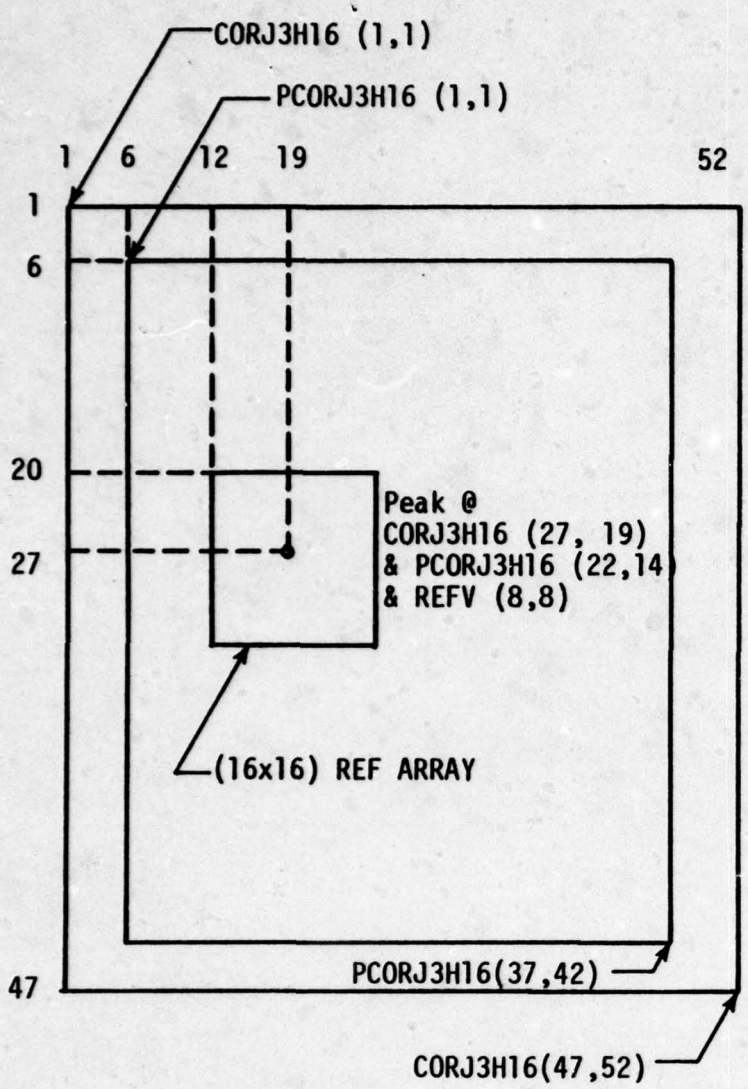

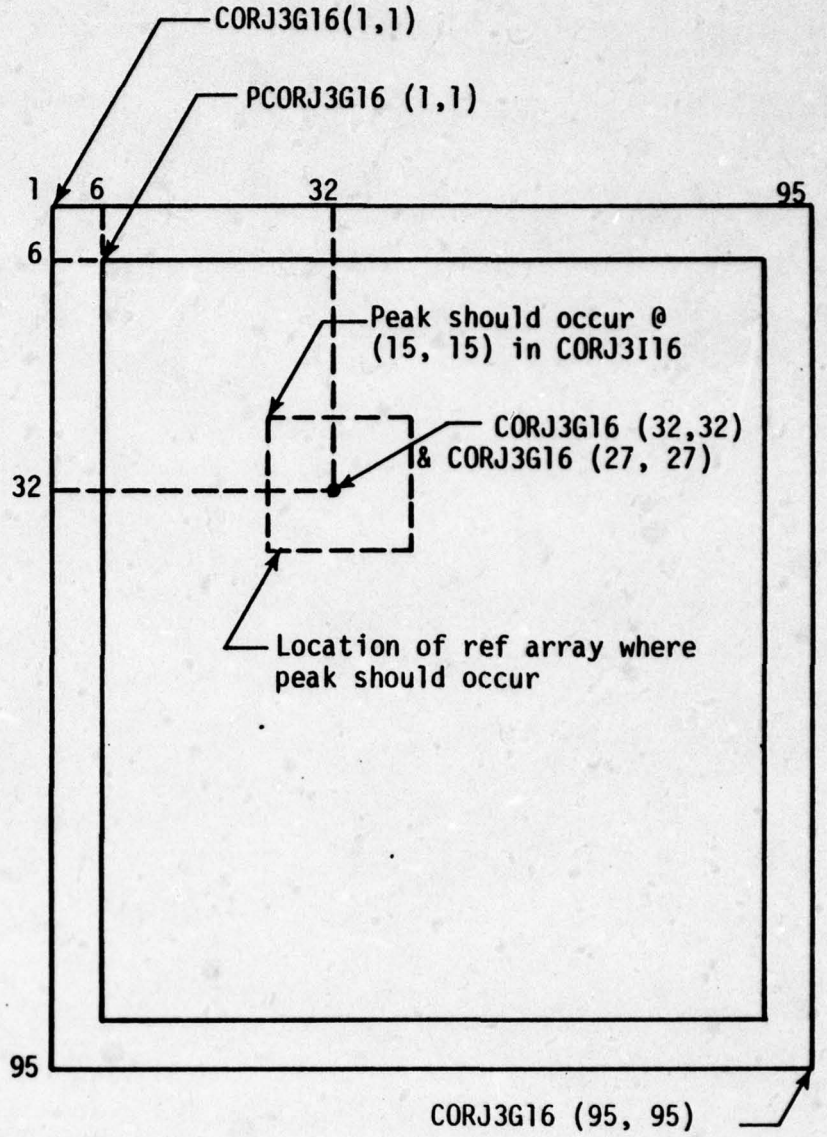

Figure 19. 16x16 autocorrelation array and expected peak.

Tables 3 through 16 give the results of simulations for seven additional scenes. A total of eight scenes was used in order to obtain data for a variety of different backgrounds. In obtaining the original eight scenes, an effort was made to include backgrounds with high spatial frequency content and with low spatial frequency content and to include scenes with both high and low contrast ratios.

Table 17 is a description of all scenes used and Table 18 is a listing of all correlation surfaces with their description.

D. Cross Sectional Plots of Correlation Surfaces

In order to examine qualitatively the size and shape of the correlation surfaces around the true peaks and false peaks, the following cross sectional plots were obtained for two scenes (parking lot and jeep in front of the fence). Figures included in this section are the cross sectional plots of the correlation surface EED28.CORJ3G32 for the jeep in front of the fence scene. In the figures (IMAX, JMAX) is the location of the first peak in the correlation surface and (IMAX1, JMAX1) is the location of the second highest peak in the correlation surface.

Figure 20 shows the cross-sectional plots through (IMAX, JMAX) of the correlation surface. Figures 21 and 22 are the cross sectional plots through (IMAX-2, JMAX-2) and (IMAX+2, JMAX+2). Similarly, Figures 23 - 26 show the cross sectional plots through (IMAX1, JMAX1) (IMAX1-2, JMAX1-2) and (IMAX1+2, JMAX1+2), respectively. Plots of third and fourth highest peaks are not included. Similar plots for other correlation surfaces listed in Table 1 and Table 2 of the previous section were obtained but are not included in this report.

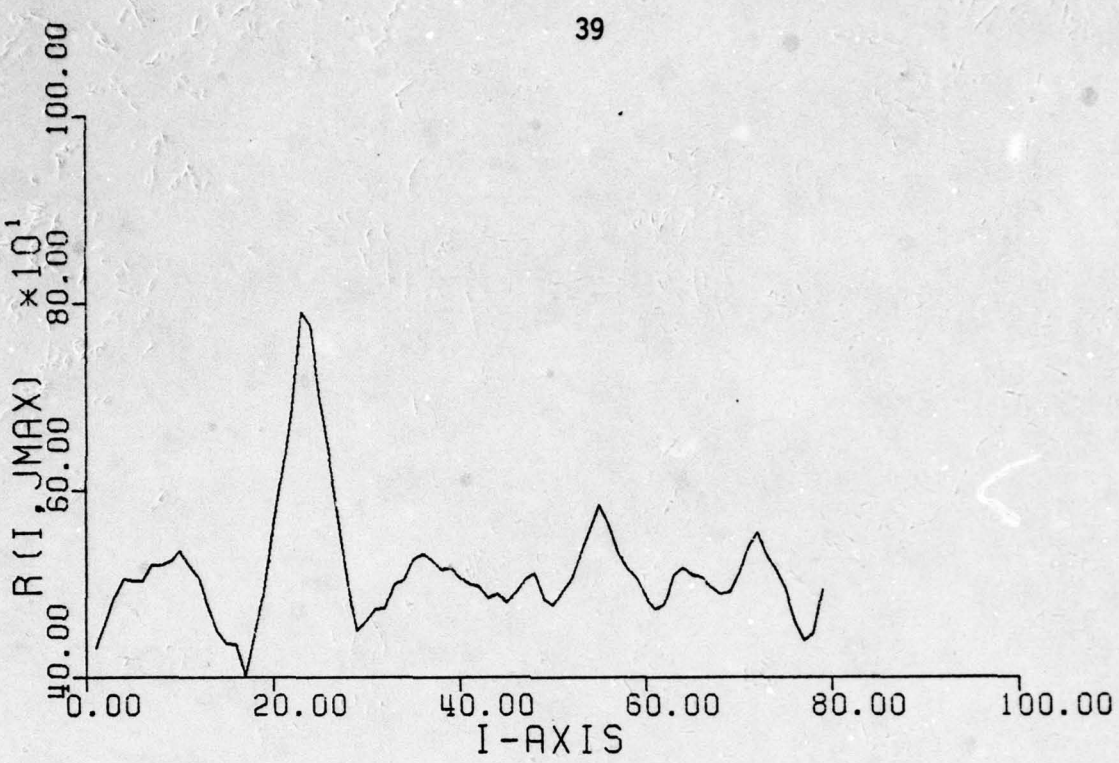

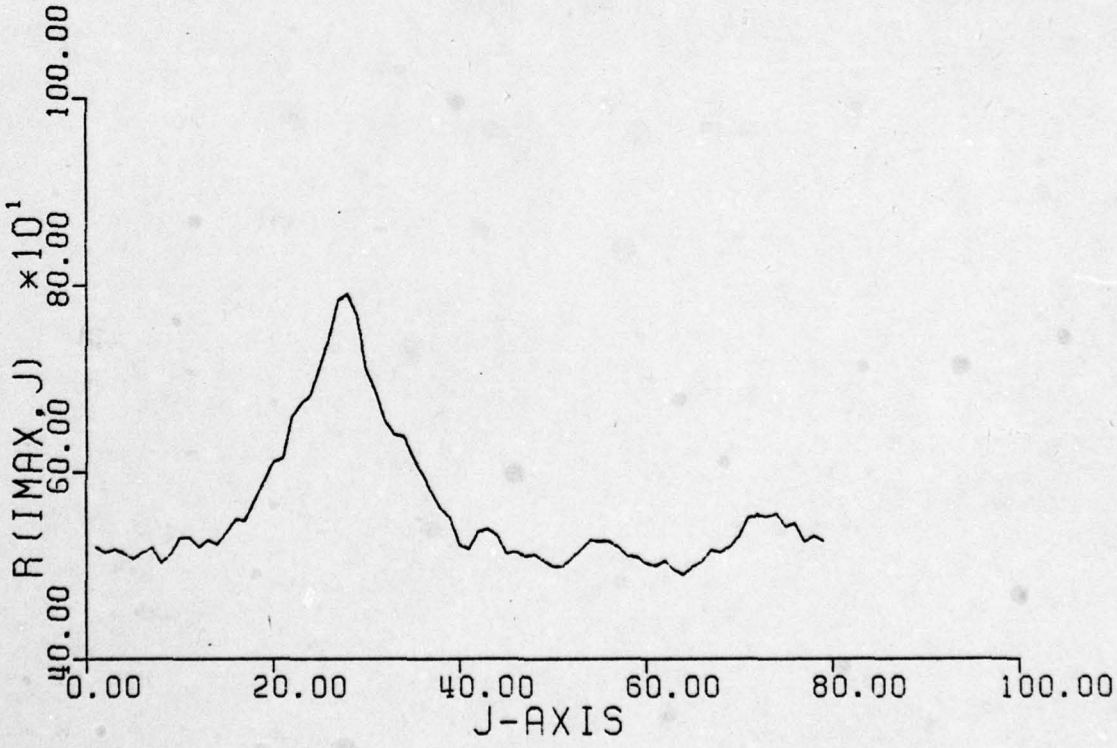

Figure 20. Cross sectional plots through (IMAX, JMAX).

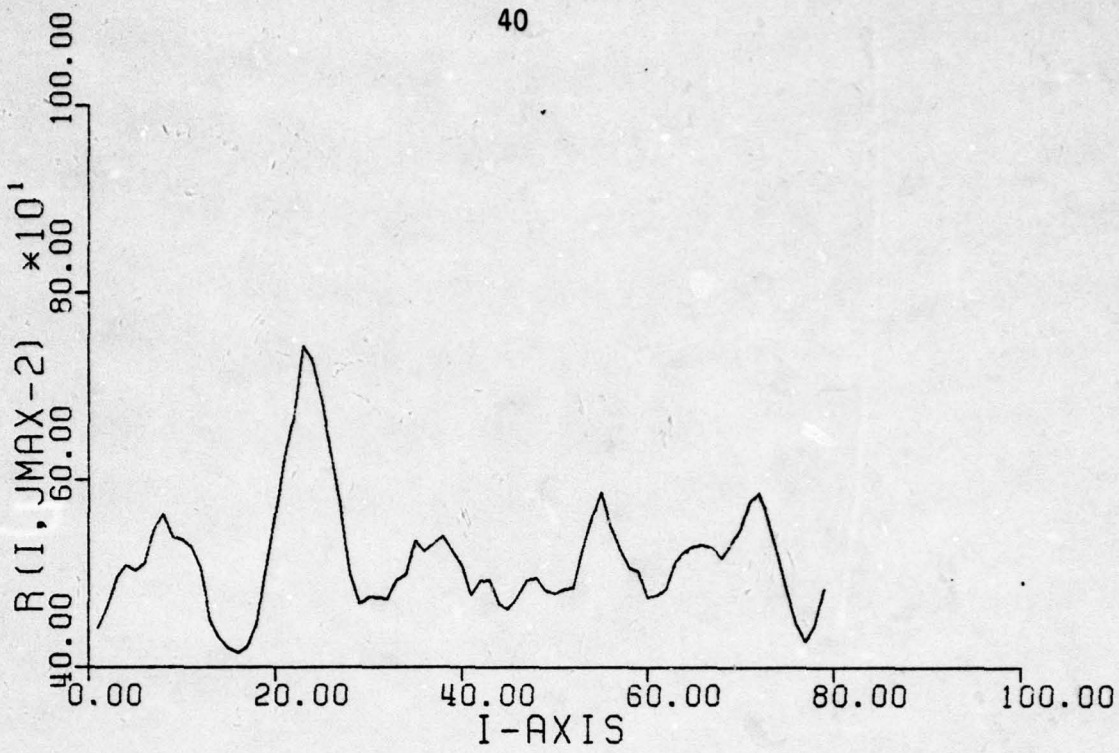

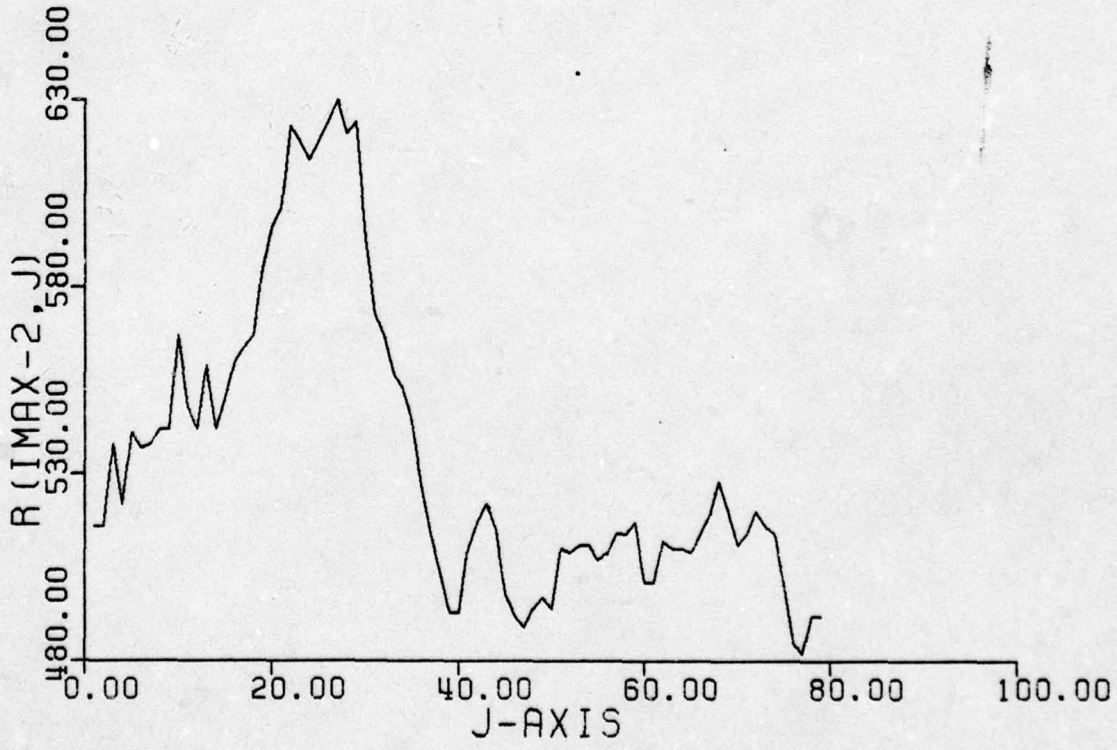

Figure 21. Cross sectional plots through (IMAX-2, JMAX-2).

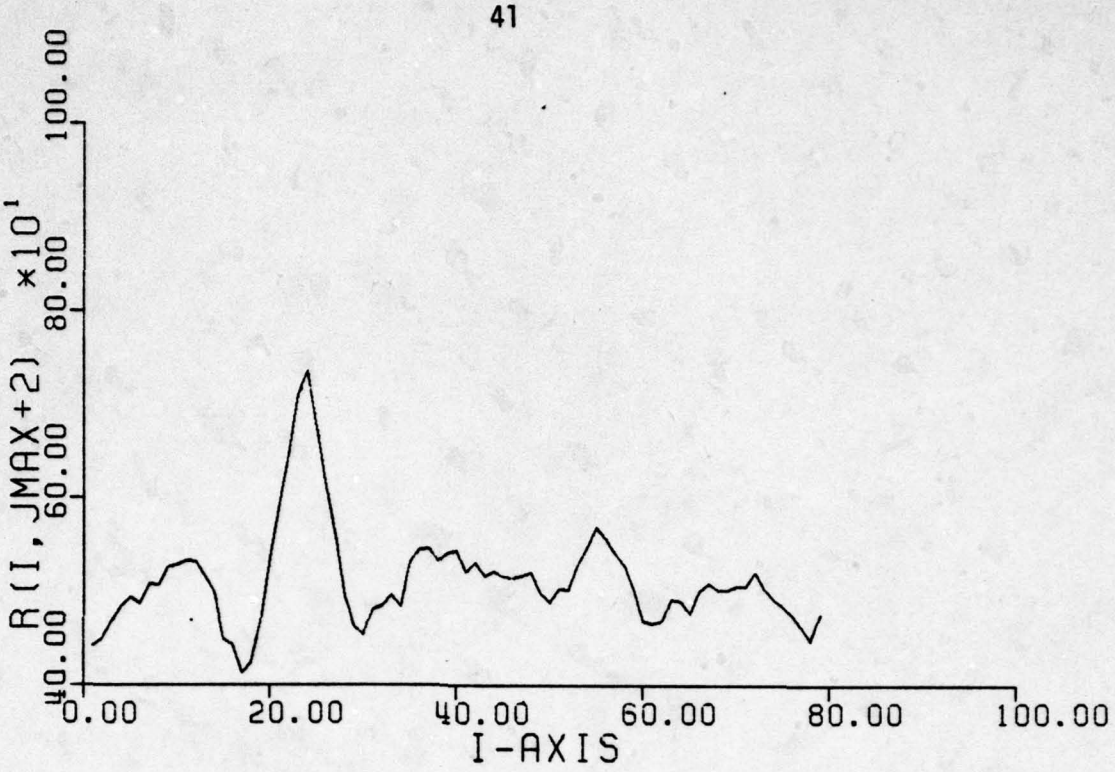

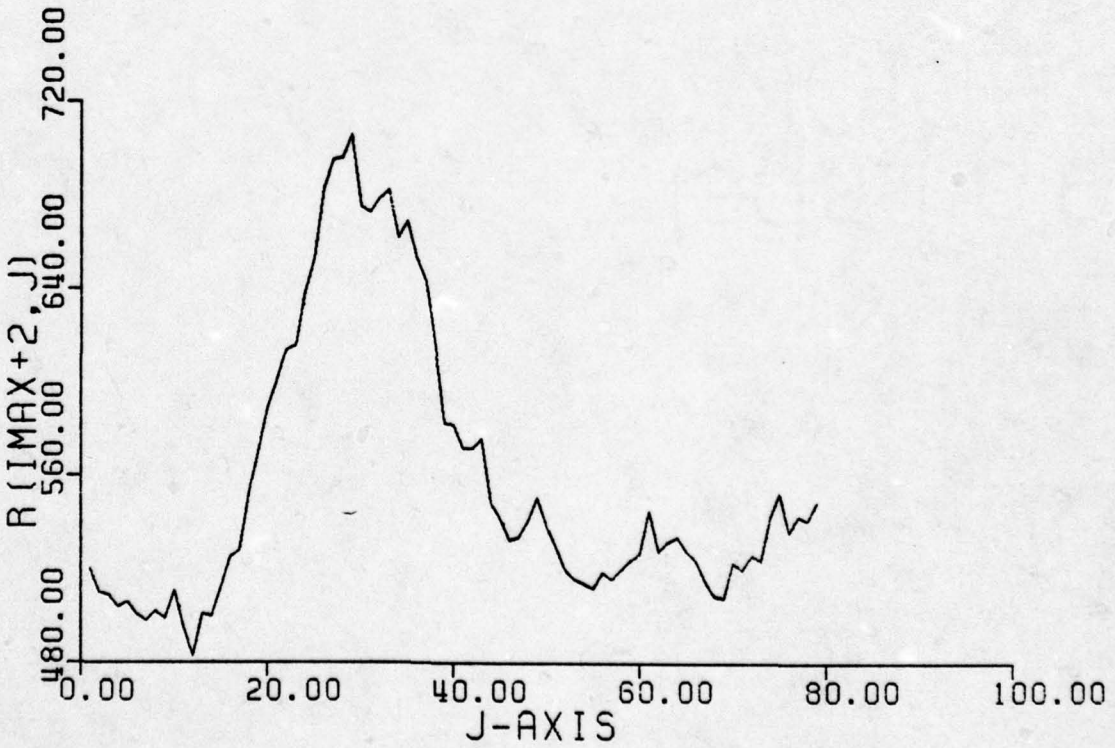

Figure 22. Cross sectional plots through (IMAX+2, JMAX+2).

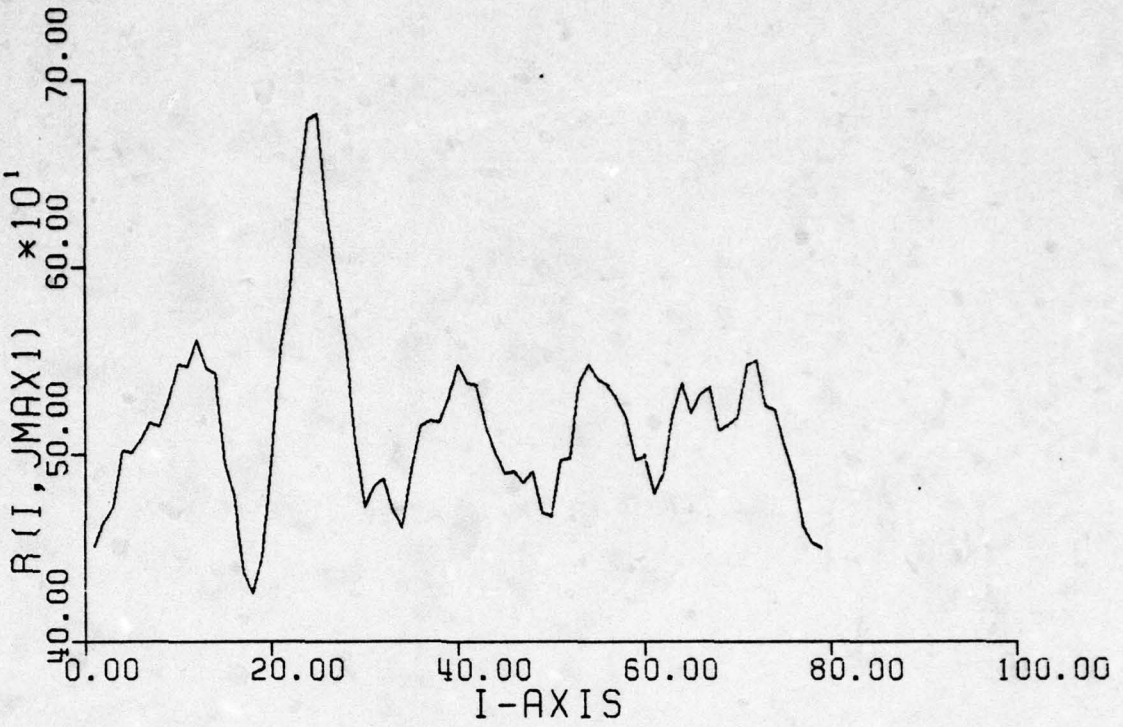

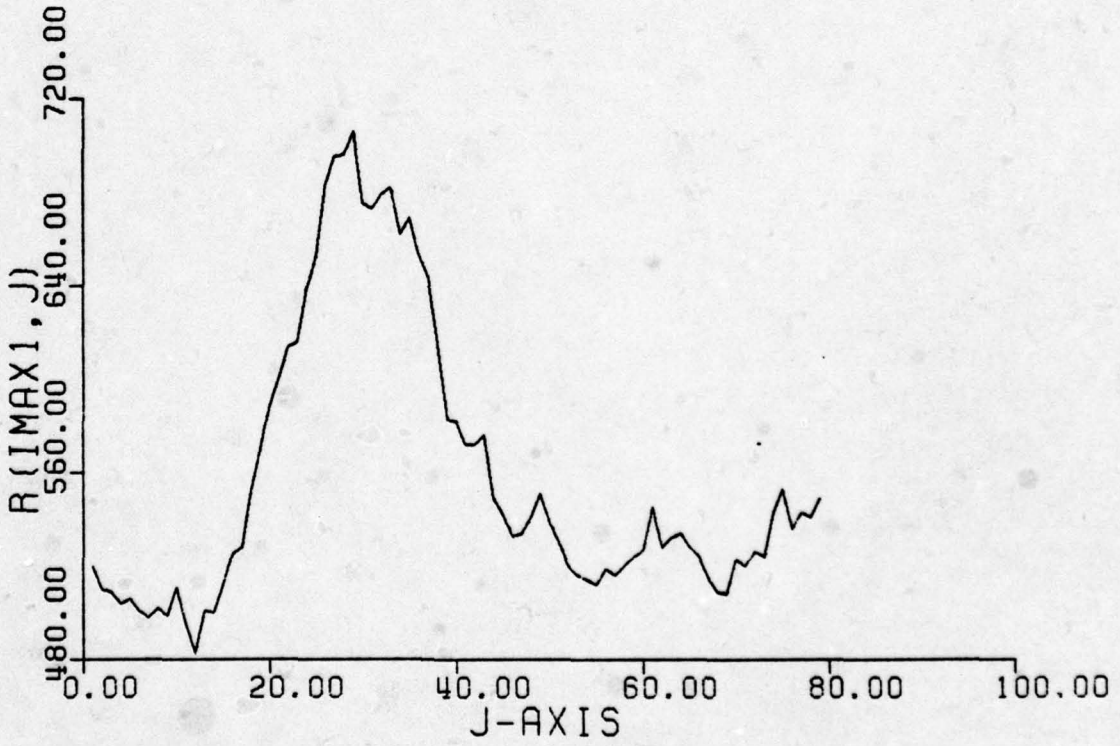

Figure 23. Cross sectional plots through (IMAX1, JMAX1).

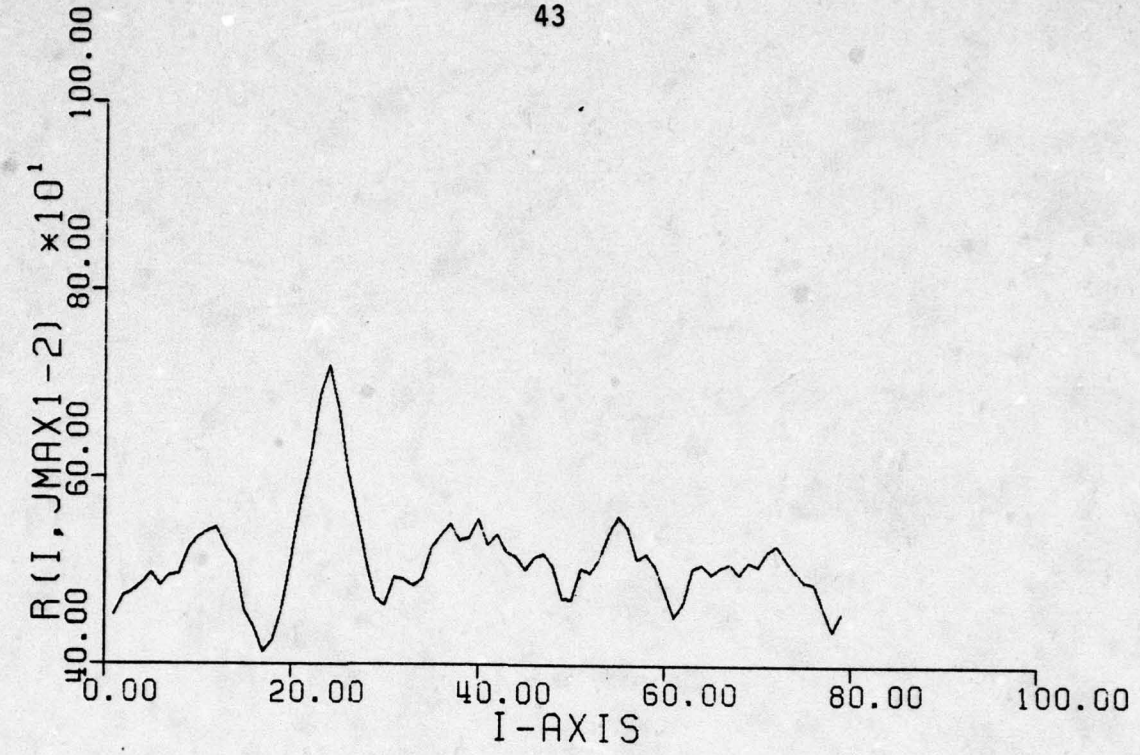

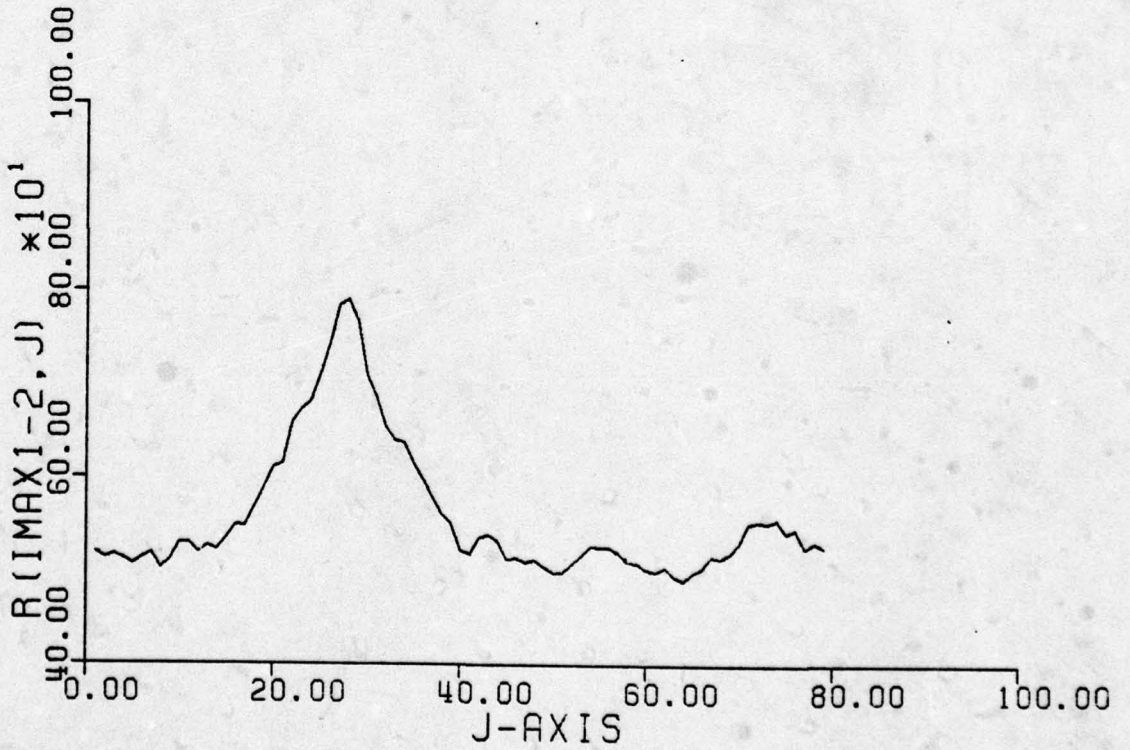

Figure 24. Cross sectional plots through (IMAX1-2, JMAX1-2).

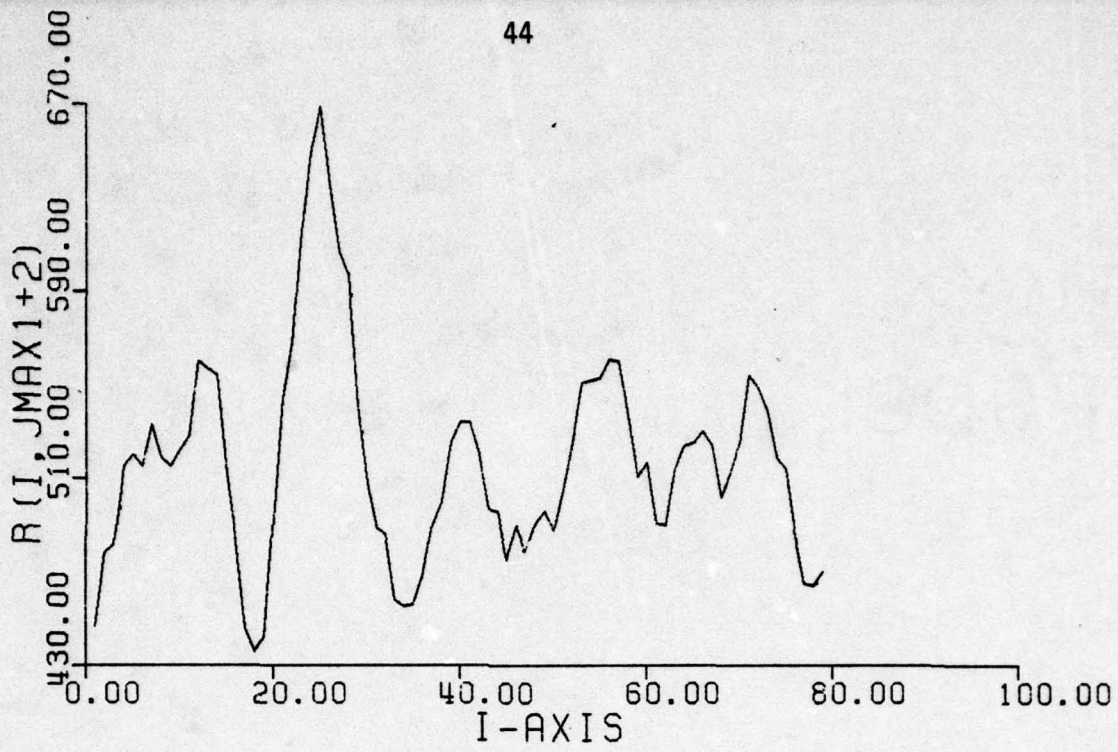

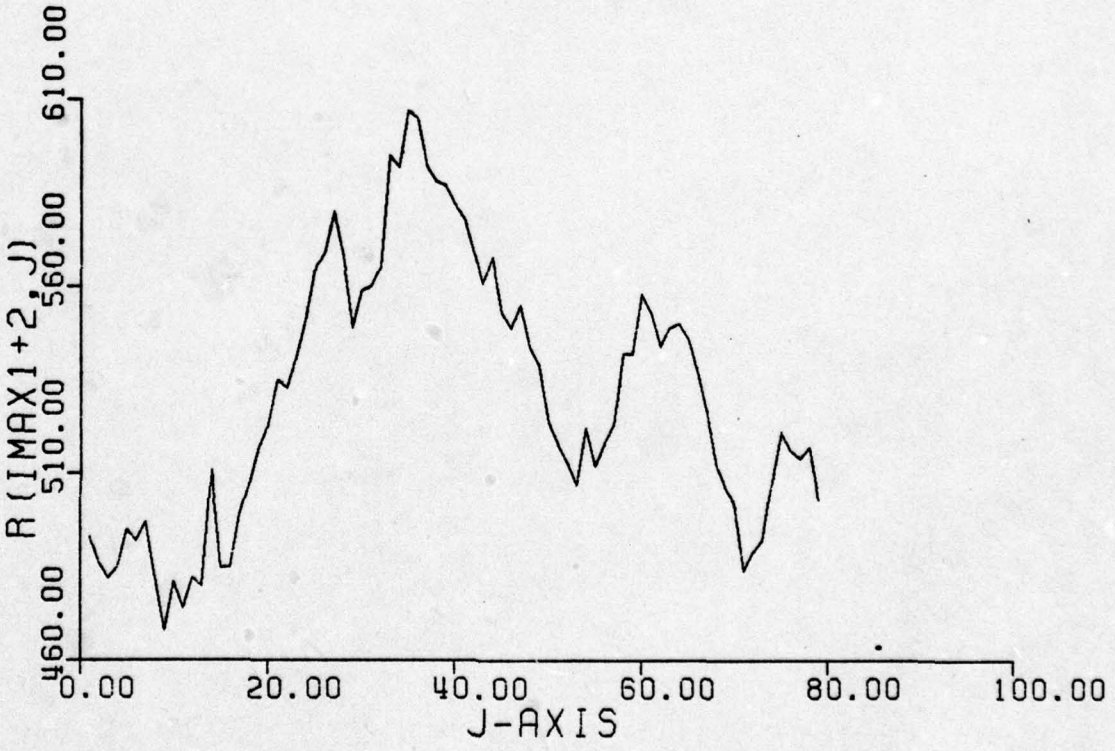

Figure 25. Cross sectional plots through (IMAX1+2, JMAX1+2).

Table 1. Scene 3 - Jeep in front of the fence, 32 x 32 reference array.

Correlation Surface	Expected Peak Location	Highest Peak & Location	Average Value of Corr. Surface	Standard Deviation of Corr. Surface	S/N Ratio	Second Highest Peak & Location	Third Highest Peak & Location	Fourth Highest Peak & Location
EED28.CORJ3A32	(23, 26)	777 (23, 28)	514.428	40.224	6.528	667 (20, 23)	631 (77, 66)	625 (3, 5)
EED28.CORJ3B32	(8, 14)	739 (8, 15)	416.629	107.196	3.007	660 (12, 20)	633 (44, 32)	629 (5, 10)
EED28.CORJ3D32	(23, 29)	714 (24, 28)	545.880	58.313	2.883	689 (16, 59)	687 (1, 70)	677 (59, 41)
EED28.CORJ3F32	(8, 14)	873 (58, 54)	588.257	88.902	3.203	825 (7, 10)	790 (53, 56)	777 (6, 55)
EED28.CORJ3G32	(23, 26)	790 (23, 28)	514.545	40.655	6.775	682 (25, 33)	673 (23, 23)	650 (13, 55)
EED28.CORJ3I32	(6, 14)	496 (6, 15)	270.156	89.917	2.512	472 (18, 7)	466 (25, 27)	459 (5, 10)

Table 2. Scene 3 - Jeep in front of the fence, 16 x 16 reference array.

Correlation Surface	Expected Peak Location	Highest Peak & Location	Average Value of Corr. Surface	Standard Deviation of Corr. Surface	S/N Ratio	Second Highest Peak & Location	Third Highest Peak & Location	Fourth Highest Peak & Location
EED28.CORJ3A16	(37, 27)	207 (38, 30)	127.655	21.088	3.763	193 (5, 17)	192 (14, 40)	189 (94, 73)
EED28.CORJ3C16	(30, 14)	226 (30, 15)	127.192	37.22	2.655	219 (41, 30)	219 (25, 19)	213 (20, 31)
EED28.CORJ3D16	(37, 37)	191 (14, 78)	125.853	20.012	3.255	188 (38, 38)	186 (43, 44)	185 (29, 60)
EED28.CORJ3F16	(30, 30)	232 (21, 46)	127.243	38.312	2.734	230 (32, 81)	226 (76, 85)	224 (22, 51)
EED28.CORJ3G16	(32, 32)	223 (33, 35)	127.150	20.294	4.723	205 (23, 61)	196 (34, 40)	195 (23, 45)
EED28.CORJ3I16	(15, 15)	215 (16, 18)	128.414	30.203	2.867	205 (63, 13)	196 (18, 24)	193 (30, 70)

Table 3. Scene 4 - Jeep behind the fence, 32 x 32 reference array.

Correlation Surface	Expected Peak Location	Highest Peak & Location	Average Value of Corr. Surface	Standard Deviation of Corr. Surface	S/N Ratio	Second Highest Peak & Location	Third Highest Peak & Location	Fourth Highest Peak & Location
EED28.CORJ4A32	(39, 37)	743 (39, 37)	505.658	42.346	5.605	650 (27, 59)	648 (8, 56)	640 (13, 30)
EED28.CORJ4C32	(26, 15)	712 (26, 14)	410.996	81.325	3.701	599 (1, 9)	594 (13, 36)	589 (42, 38)
EED28.CORJ4D32	(39, 37)	763 (19, 84)	545.685	72.044	3.016	747 (39, 37)	725 (1, 62)	724 (13, 22)
EED28.CORJ4F32	(26, 22)	788 (27, 20)	536.186	109.147	2.307	776 (14, 41)	770 (56, 55)	763 (26, 15)
EED28.CORJ4G32	(44, 42)	800 (45, 42)	506.467	40.542	7.240	701 (45, 47)	689 (45, 37)	686 (46, 8)
EED28.CORJ4I32	(26, 15)	507 (28, 2)	271.310	93.639	2.517	492 (27, 15)	486 (27, 20)	481 (28, 7)

Table 4. Scene 4 - Jeep behind the fence, 16 x 16 reference array.

Correlation Surface	Expected Peak & Location	Highest Peak & Location	Average Value of Corr. Surface	Standard Deviation of Corr. Surface	S/N Ratio	Second Highest Peak & Location	Third Highest Peak & Location	Fourth Highest Peak & Location
EED28.CORJ4A16	(47, 48)	191 (47, 49)	128.652	14.568	4.280	180 (63, 33)	175 (21, 43)	172 (6, 69)
EED28.CORJ4C16	(40, 31)	209 (40, 31)	127.609	24.857	3.274	198 (49, 48)	198 (25, 12)	193 (45, 40)
EED28.CORJ4D16	(47, 48)	215 (47, 49)	133.035	21.292	3.850	206 (61, 16)	197 (94, 101)	196 (39, 80)
EED28.CORJ4F16	(40, 41)	227 (87, 89)	126.876	36.667	2.731	217 (30, 62)	214 (33, 69)	213 (37, 17)
EED28.CORJ4G16	(52, 53)	201 (53, 54)	127.023	17.162	4.311	192 (40, 43)	179 (28, 8)	178 (54, 26)
EED28.CORJ4I16	(40, 38)	219 (52, 20)	129.057	38.421	2.341	215 (25, 67)	215 (25, 52)	211 (42, 21)

Table 5. Scene 2 - Jeep in the parking lot, 32 x 32 reference array.

Correlation Surface	Expected Peak Location	Highest Peak & Location	Average Value of Corr. Surface	Standard Deviation of Corr. Surface	S/N Ratio	Second Highest Peak & Location	Third Highest Peak & Location	Fourth Highest Peak & Location
EED28.CORJ2A32	(30, 44)	751 (30, 44)	511.581	43.644	5.486	636 (36, 46)	627 (43, 11)	625 (60, 79)
EED28.CORJ2C32	(15, 19)	694 (16, 20)	411.338	88.954	3.191	626 (21, 21)	609 (58, 35)	609 (11, 18)
EED28.CORJ2D32	(30, 54)	839 (30, 53)	509.992	71.226	4.620	754 (44, 18)	736 (29, 48)	730 (45, 75)
EED28.CORJ2F32	(15, 30)	767 (21, 31)	433.998	158.807	2.097	746 (55, 17)	741 (50, 14)	737 (21, 36)
EED28.CORJ2G32	(25, 49)	754 (24, 49)	511.150	48.062	5.053	671 (24, 44)	664 (25, 27)	653 (10, 6)
EED28.CORJ2I32	(11, 19)	498 (11, 20)	273.488	106.149	2.115	486 (12, 35)	485 (24, 39)	483 (23, 32)

Table 6. Scene 2 - Jeep in the parking lot, 16 x 16 reference array.

Correlation Surface	Expected Peak Location	Highest Peak & Location	Average Value of Corr. Surface	Standard Deviation of Corr. Surface	S/N Ratio	Second Highest Peak & Location	Third Highest Peak & Location	Fourth Highest Peak & Location
EED28.CORJ2A16	(41, 50)	218 (40, 50)	127.932	23.532	3.827	202 (75, 35)	197 (64, 30)	194 (53, 19)
EED28.CORJ2C16	(34, 33)	235 (68, 18)	126.998	41.833	2.582	230 (38, 35)	225 (9, 25)	224 (46, 54)
EED28.CORJ2D16	(41, 60)	215 (41, 60)	127.853	22.367	3.896	209 (76, 45)	192 (17, 24)	189 (25, 90)
EED28.CORJ2F16	(34, 53)	223 (31, 28)	127.679	36.593	2.605	220 (43, 56)	220 (11, 17)	214 (2, 35)
EED28.CORJ2G16	(36, 55)	213 (36, 55)	127.451	20.182	4.239	193 (13, 67)	189 (12, 59)	187 (13, 75)
EED28.CORJ2I16	(24, 43)	228 (37, 13)	127.323	44.345	2.270	227 (24, 43)	218 (48, 9)	216 (10, 43)

Table 7. NASA tower, 32 x 32 reference array.

Correlation Surface	Expected Peak Location	Highest Peak & Location	Average Value of Corr. Surface	Standard Deviation of Corr. Surface	S/N Ratio	Second Highest Peak & Location	Third Highest Peak & Location	Fourth Highest Peak & Location
EED28.CORNTA32	(30, 22)	683 (31, 22)	507.304	42.950	4.091	648 (9, 41)	642 (16, 37)	630 (22, 29)
EED28.CORNTC32	(16, 10)	697 (12, 12)	427.342	116.950	2.306	674 (17, 10)	668 (7, 15)	654 (13, 41)
EED28.CORNTD32	(30, 32)	776 (76, 89)	532.111	78.615	3.102	765 (76, 82)	757 (81, 85)	756 (71, 83)
EED28.CORNTF32	(16, 17)	750 (30, 36)	509.409	91.515	2.626	721 (1, 13)	717 (35, 34)	696 (25, 36)
EED28.CORNTG32	(25, 27)	662 (26, 28)	511.282	55.609	5.885	592 (8, 30)	589 (78, 75)	589 (26, 66)
EED28.CORNTI32	(16, 10)	378 (16, 10)	272.812	33.345	3.184	378 (5, 37)	372 (39, 36)	351 (6, 28)

Table 8. NASA tower, 16 x 16 reference array.

Correlation Surface	Expected Peak Location	Highest Peak & Location	Average Value of Corr. Surface	Standard Deviation of Corr. Surface	S/N Ratio	Second Highest Peak & Location	Third Highest Peak & Location	Fourth Highest Peak & Location
EED28.CORNTA16	(33, 21)	208 (105, 77)	128.565	21.873	3.632	206 (34, 22)	205 (12, 43)	199 (19, 38)
EED28.CORNTC16	(26, 9)	242 (7, 29)	129.079	47.989	2.353	233 (6, 8)	231 (12, 26)	230 (31, 40)
EED28.CORNTD16	(33, 32)	239 (102, 86)	132.494	28.372	3.754	232 (97, 88)	232 (71, 89)	220 (28, 34)
EED28.CORNTF16	(26, 25)	222 (61, 35)	127.053	32.465	2.925	214 (87, 30)	209 (28, 7)	207 (66, 33)
EED28.CORNTG16	(28, 27)	189 (29, 28)	127.600	13.398	4.583	175 (92, 62)	171 (27, 91)	170 (27, 42)
EED28.CORNTI16	(16, 15)	202 (17, 15)	127.062	25.204	2.973	197 (42, 64)	193 (70, 62)	192 (25, 62)

Table 9. Woods scene, 32 x 32 reference array.

Correlation Surface	Expected Peak Location	Highest Peak & Location	Average Value of Corr. Surface	Standard Deviation of Corr. Surface	S/N Ratio	Second Highest Peak & Location	Third Highest Peak & Location	Fourth Highest Peak & Location
EED28.CORWDA32	(28, 21)	770 (28, 21)	508.721	53.167	4.914	682 (22, 23)	657 (55, 47)	656 (49, 51)
EED28.CORWDC32	(13, 8)	733 (13, 8)	420.701	87.457	3.571	631 (8, 8)	630 (34, 36)	629 (18, 9)
EED28.CORWDD32	(28, 31)	753 (27, 30)	522.385	69.483	3.319	697 (38, 28)	693 (31, 25)	677 (1, 89)
EED28.CORWDF32	(13, 16)	820 (58, 48)	547.774	113.147	2.406	803 (1, 10)	749 (53, 49)	740 (6, 12)
EED28.CORWDG32	(23, 26)	745 (23, 27)	510.797	30.741	7.619	609 (39, 41)	606 (22, 10)	604 (58, 19)
EED28.CORWDI32	(11, 8)	443 (11, 8)	273.578	53.965	3.141	406 (2, 29)	395 (22, 1)	386 (45, 10)

Table 10. Woods scene, 16 x 16 reference array.

Correlation Surface	Expected Peak Location	Highest Peak & Location	Average Value of Corr. Surface	Standard Deviation of Corr. Surface	S/N Ratio	Second Highest Peak & Location	Third Highest Peak & Location	Fourth Highest Peak & Location
EED28.CORWDA16	(36, 29)	196 (58, 55)	126.534	23.391	2.970	193 (37, 39)	192 (79, 2)	190 (32, 4)
EED28.CORWDC16	(29, 12)	242 (81, 16)	128.340	57.105	2.224	241 (33, 47)	237 (28, 48)	237 (21, 13)
EED28.CORWDD16	(36, 39)	188 (63, 76)	126.967	18.460	3.306	183 (21, 88)	182 (34, 72)	181 (69, 7)
EED28.CORWDF16	(29, 24)	227 (29, 8)	124.107	37.595	2.737	226 (50, 90)	222 (55, 15)	219 (48, 85)
EED28.CORWDG16	(31, 34)	195 (31, 35)	127.117	15.832	4.288	186 (45, 39)	176 (65, 39)	176 (65, 29)
EED28.CORWDI16	(19, 22)	216 (18, 4)	127.088	30.066	2.957	214 (9, 42)	208 (51, 29)	206 (18, 21)

Table 11. Water tower, 32 x 32 reference array.

Correlation Surface	Expected Peak Location	Highest Peak & Location	Average Value of Corr. Surface	Standard Deviation of Corr. Surface	S/N Ratio	Second Highest Peak & Location	Third Highest Peak & Location	Fourth Highest Peak & Location
EED28.CORWTA32	(33, 23)	703 (32, 23)	506.882	31.545	6.217	640 (37, 25)	615 (27, 26)	599 (49, 24)
EED28.CORWTC32	(18, 10)	706 (18, 9)	425.563	129.364	2.168	674 (26, 4)	671 (13, 9)	661 (24, 9)
EED28.CORWTD32	(33, 33)	730 (33, 30)	521.356	56.491	3.698	712 (47, 24)	664 (55, 24)	657 (11, 86)
EED28.CORWTF32	(18, 18)	905 (18, 11)	542.783	137.553	2.633	899 (13, 13)	857 (23, 10)	828 (8, 14)
EED28.CORWTG32	(28, 28)	683 (28, 27)	510.261	24.077	7.175	594 (50, 56)	589 (66, 59)	535 (2, 50)
EED28.CORWTI32	(11, 10)	384 (11, 9)	272.315	44.369	2.517	380 (19, 9)	379 (2, 18)	377 (34, 18)

Table 12. Water tower, 16 x 16 reference array.

Correlation Surface	Expected Peak Location	Highest Peak & Location	Average Value of Corr. Surface	Standard Deviation of Corr. Surface	S/N Ratio	Second Highest Peak & Location	Third Highest Peak & Location	Fourth Highest Peak & Location
ED28.CORWTA16	(37, 30)	194 (37, 30)	127.716	13.446	4.930	181 (32, 37)	180 (103, 48)	178 (28, 58)
ED28.CORWTC16	(30, 13)	217 (69, 23)	127.289	30.934	2.900	217 (32, 14)	211 (90, 32)	209 (72, 47)
ED28.CORWTD16	(37, 40)	197 (37, 35)	127.306	16.092	4.331	192 (37, 40)	183 (33, 48)	175 (28, 64)
ED28.CORWTF16	(30, 33)	224 (14, 71)	132.475	34.288	2.669	219 (6, 57)	217 (37, 10)	215 (8, 52)
ED28.CORWTG16	(32, 35)	179 (32, 34)	128.712	14.318	3.512	177 (8, 23)	173 (54, 83)	170 (53, 68)
ED28.CORWTI16	(20, 23)	235 (50, 60)	126.837	43.361	2.494	227 (20, 22)	226 (51, 51)	224 (28, 21)

^
FED28

Table 13. Rock quarry, 32 x 32 reference array.

Correlation Surface	Expected Peak Location	Highest Peak & Location	Average Value of Corr. Surface	Standard Deviation of Corr. Surface	S/N Ratio	Second Highest Peak & Location	Third Highest Peak & Location	Fourth Highest Peak & Location
EED28.CORRQA32	(36, 57)	760 (36, 57)	512.088	42.173	5.878	669 (81, 36)	636 (10, 59)	626 (61, 57)
EED28.CORRQC32	(21, 33)	693 (21, 33)	420.782	72.514	3.754	597 (15, 1)	584 (16, 36)	578 (10, 35)
EED28.CORRQD32	(36, 67)	724 (36, 66)	503.699	57.752	3.815	688 (82, 42)	671 (59, 89)	669 (81, 47)
EED28.CORRQF32	(20, 35)	759 (2, 24)	522.656	117.345	2.014	740 (47, 25)	735 (54, 24)	731 (5, 19)
EED28.CORRQG32	(31, 62)	723 (31, 62)	512.722	25.654	8.197	607 (64, 75)	596 (6, 66)	595 (63, 1)
EED28.CORRQI32	(12, 33)	384 (12, 33)	272.379	34.640	3.222	362 (19, 20)	361 (30, 40)	355 (25, 32)

Table 14. Rock quarry, 16 x 16 reference array.

Correlation Surface	Expected Peak Location	Highest Peak & Location	Average Value of Corr. Surface	Standard Deviation of Corr. Surface	S/N Ratio	Second Highest Peak & Location	Third Highest Peak & Location	Fourth Highest Peak & Location
EED28.CORRQA16	(40, 72)	171 (40, 71)	128.360	11.744	3.631	168 (31, 6)	164 (76, 50)	164 (60, 22)
EED28.CORRQC16	(33, 55)	215 (56, 2)	127.727	32.064	2.722	213 (33, 55)	209 (64, 24)	206 (60, 13)
EED28.CORRQD16	(40, 82)	171 (29, 20)	128.109	11.334	3.784	169 (99, 50)	166 (65, 26)	165 (37, 62)
EED28.CORRQF16	(33, 72)	197 (47, 14)	127.637	21.467	3.231	192 (50, 80)	188 (35, 12)	186 (63, 41)
EED28.CORRQG16	(35, 77)	180 (35, 77)	128.388	12.399	4.163	172 (89, 18)	170 (9, 81)	169 (68, 90)
EED28.CORRQI16	(23, 65)	152 (22, 65)	94.840	19.845	2.880	149 (45, 13)	144 (38, 7)	142 (63, 52)

Table 15. Parking lot, 32 x 32 reference array.

Correlation Surface	Expected Peak Location	Highest Peak & Location	Average Value of Corr. Surface	Standard Deviation of Corr. Surface	S/N Ratio	Second Highest Peak & Location	Third Highest Peak & Location	Fourth Highest Peak & Location
ED28.CORR4A32	(28, 35)	785 (28, 35)	512.512	42.310	6.440	655 (60, 45)	Not Obtained	Not Obtained
ED28.CORR4C32	(13, 8)	684 (12, 9)	410.505	88.998	3.073	613 (54, 22)	Not Obtained	Not Obtained
ED28.CORR4D32	(28, 35)	742 (28, 34)	525.466	45.39	4.771	649 (32, 5)	643 (28, 39)	642 (63, 71)
ED28.CORR4F32	(13, 20)	710 (55, 1)	514.696	69.794	2.798	707 (50, 1)	702 (35, 32)	687 (29, 28)
ED28.CORR4G32	(28, 35)	860 (28, 36)	510.164	57.723	6.061	743 (28, 31)	696 (27, 41)	693 (28, 24)
ED28.CORR4I32	(9, 8)	514 (10, 1)	226.335	116.324	2.129	512 (9, 16)	507 (8, 31)	505 (9, 22)

Table 16. Parking lot, 16 x 16 reference array.

Correlation Surface	Expected Peak Location	Highest Peak & Location	Average Value of Corr. Surface	Standard Deviation of Corr. Surface	S/N Ratio	Second Highest Peak & Location	Third Highest Peak & Location	Fourth Highest Peak & Location
ED28.CORR4A16	(48, 47)	206 (48, 48)	128.138	18.343	4.245	196 (46, 22)	Not Obtained	Not Obtained
ED28.CORR4C16	(40, 29)	213 (40, 3)	127.698	31.277	2.727	211 (40, 31)	Not Obtained	Not Obtained
ED28.CORR4D16	(28, 35)	201 (30, 16)	132.123	20.943	3.298	197 (47, 85)	193 (12, 23)	192 (47, 90)
ED28.CORR4F16	(40, 39)	160 (40, 41)	89.121	23.766	2.982	150 (42, 12)	Not Obtained	Not Obtained
ED28.CORR4G16	(28, 35)	216 (28, 36)	127.717	23.715	3.680	203 (40, 68)	200 (28, 31)	198 (47, 85)
ED28.CORR4I16	(16, 23)	226 (17, 4)	128.379	50.234	1.943	225 (4, 51)	224 (45, 67)	224 (16, 23)

Table 17. Description of scenes.

EED28.CORNTXXX - NASA tower.

CORWTXXX - Water tower.

CORWDXXX - Woods.

CORR4XXX - Parking lot.

CORRQXXX - Rock quarry.

CORJ2XXX - Jeep in the parking lot.

CORJ3XXX - Jeep in front of the fence.

CORJ4XXX - Jeep behind the fence.

Table 18. Description of correlation surfaces.

EED28.CORXXA32 - Cross correlation of PLRV with REFV of size 32 x 32 from PHRV using digital line average quantizer.

B32 - Autocorrelation of PHRV with REFV of size 32 x 32 from PHRV itself using digital line average quantizer.

C32 - Correlation of the correlation surface A with REFV of size 32 x 26 from correlation surface B using digital line average quantizer.

D32 - Cross Correlation of PLRV with REFV of size 32 x 32 from PHRV using analog filter quantizer.

E32 - Autocorrelation of PHRV with REFV of size 32 x 32 from PHRV itself using analog filter quantizer.

F32 Correlation of correlation surface D with REFV of size 32 x 32 from correlation surface E using analog filter quantizer.

G32 - Cross correlation of PLRV with REFV of size 32 x 32 from PHRV using area average quantizer.

H32 - Autocorrelation of PHRV with REFV of size 32 x 32 from PHRV itself using area average quantizer.

I32 - Correlation of correlation surface G with REFV of size 21 x 26 from correlation surface H using area average quantizer.

Table 18. Description of correlation surfaces.

A16 - Cross correlation of PLRV with REFV of size 16 x 16 from PHRV using digital line average quantizer.

B16 - Autocorrelation of PHRV with REFV of size 16 x 16 from PHRV itself using digital line average quantizer.

C16 - Correlation of the correlation surface A with REFV of size 16 x 16 from correlation surface B using digital line average quantizer.

D16 - Cross correlation of PLRV with REFV of size 16 x 16 from PHRV using analog filter quantizer.

E16 - Autocorrelation of PHRV with REFV of size 16 x 16 from PHRV itself using analog filter quantizer.

F16 - Correlation of correlation surface D with REFV of size 16 x 16 from correlation surface E using analog filter quantizer.

G16 - Cross correlation of PLRV with REFV of size 16 x 16 from PHRV using area average quantizer.

H16 - Autocorrelation of PHRV with REFV of size 16 x 16 from PHRV itself using area average quantizer.

I16 - Correlation of correlation surface G with REFV of size 16 x 16 from correlation surface H using area average quantizer.

3. CONCLUSIONS

In this chapter, the relative performance of the three quantizers based on the simulation results of the eight different scenes listed in the previous chapter are presented.

1. It was mentioned earlier that an equal number of 'zeros' and 'ones' in the REFV is essential for better correlation results. It was found that the area average quantizer needs fewer iterations to yield an equal number of zeros and ones in REFV when compared to the line average quantizer and the analog filter quantizer for a given scene. The analog filter quantizer needs a significantly larger number of iterations when compared to the other two quantizers.

2. The area average quantizer identifies the true location of the target in all eight scenes for a REFV of size 32 x 32 as well as 16 x 16. The line average quantizer identifies the true location of the target in all eight scenes for REFV of size 32 x 32; but when REFV of size 16 x 16 is used it identifies the target for only six of the eight scenes. However, the true peak appears as the second highest peak in the correlation surfaces for the other two scenes. When the analog filter quantizer is used with REFV of size 32 x 32, the true location of the target is identified in six scenes and the true peak appears as the second highest peak in the correlation surface for one of the other scenes. When a REFV of size 16 x 16 is used, the target was correctly identified in only two of the eight scenes. In two more scenes the true peak

appears as the second highest peak in the correlation surfaces. The target was not found in the remaining four scenes. This clearly shows the superiority of the area average quantizer over the other two quantizers.

3. In most of the correlation surfaces,

$$(\text{S/N ratio})_{\text{Area avg.}} > (\text{S/N ratio})_{\text{Line avg.}} > (\text{S/N ratio})_{\text{Analog filter}}$$

4. The correlation surfaces labeled C in Tables 1 - 16 were obtained by correlating a reference array obtained from the B surface with the A surface. The B surfaces, which are not included in Tables 1 - 16, were obtained by correlating a 32 x 32 or 16 x 16 reference from the processed high resolution video (PHRV) with the PHRV, yielding a quasi-autocorrelation surface. The idea being that if the processed HR video and processed LR video are close to being identical (i.e., the ideal case) then autocorrelation of a reference taken out of PHRV with the PHRV should yield a correlation surface very close to the cross-correlation of the PHRV with PLRV. Then by choosing a reference from surface B centered about the autocorrelation peak and correlating with surface A, one should obtain the location of the true peak in A even if it is not the highest peak in the surface.

The above approach was motivated by the need to establish some criterion, based on the shape of the correlation surface about the peak, for picking out the true correlation peak in a correlation surface even though it may not be the highest peak. Upon observing many correlation surfaces, this author came to the conclusion that the shape of the

correlation surface about the true peak is quite different for various scenes and therefore cannot be characterized very well by one or more surface shape criteria.

Similarly, surfaces F and I in Tables 1 - 16 were obtained by taking the reference from surfaces E and H and correlating with surfaces D and G, respectively.

From Tables 1 - 16 it is clear that this approach did not yield very good results. Examination of the correlation surfaces in Figure 20 through 25 and numerous others which were generated, revealed that quite often the correlation surface about a false peak is quite similar to the shape of the surface about the true peak when quantized to only two levels. In these cases, correlation of the correlation surfaces does not yield meaningful results. Techniques such as normalization of the correlation surfaces, offsetting the value used in the two-level quantization, non-equal number of ones and zeros, etc., were tried, none of which improved the results significantly.

From the above it was concluded that correlation of the correlation surfaces is not useful in determining the true correlation peak. From the results obtained in the simulations, it is questionable whether any set of criteria, based on the expected shape of the correlation surface about a true peak, can be specified which will yield good results for all scenes.

5. Table 19 was obtained by computing the ratio of the correlation peak to the second highest peak for the A, D and G correlation surfaces in Tables 1 - 16. The astericks indicate the cases where false

correlation occurred. The digital area average (G) correlated correctly in all sixteen cases; the digital line average (A) correlated correctly in all but two cases (both were using 16 x 16 reference arrays); and the analog line averager (D) correlated correctly in 9 or the 16 cases. The digital area average had the highest peak to second peak ratio in 10 of the 16 cases and the digital line average in 6 of the 16 cases.

6. The average values of the correlation surfaces were fairly close to being the same in all cases. It is noted that the digital line and digital area average were usually the closest in value. The same is true of the correlation surface standard deviation.

Table 19. Ratio of correlation peak to second highest peak.

Table Number	A	D	G
1	1.165	1.036	1.158
2	1.073	1.016*	1.088
3	1.143	1.021*	1.141
4	1.061	1.043	1.047
5	1.181	1.113	1.124
6	1.079	1.029	1.104
7	1.054	1.014*	1.118
8	1.010*	1.030*	1.08
9	1.130	1.080	1.223
10	1.016*	1.027*	1.048
11	1.098	1.025	1.150
12	1.072	1.026	1.011
13	1.136	1.052	1.191
14	1.018	1.012*	1.046
15	1.198	1.143	1.157
16	1.051	1.020*	1.064